AD NUMBER

AD914057

LIMITATION CHANGES

TO:

Approved for public release; distribution is unlimited.

FROM:

Distribution authorized to U.S. Gov't. agencies only; Test and Evaluation; 20 NOV 1972. Other requests shall be referred to Night Vision Laboratory, Fort Belvoir, VA 22060.

AUTHORITY

AEC/NVL ltr, 12 Feb 1974

Contract No. DAAK02-72-C-0422 Effective Date 20 April 1972
Amount of Contract $29,296 Expiration Date 20 Nov 1972

DEVELOPMENT OF VARIABLE AFFINITY BARRIER PHOTOEMITTER

SPONSORED BY:

ADVANCED RESEARCH PROJECTS AGENCY
ARPA ORDER No. 2167

FINAL TECHNICAL REPORT

PREPARED BY:

BETA INDUSTRIES, INC.
DAYTON, OHIO 45429

JOHN L. MIZE
PRINCIPAL INVESTIGATOR & PROJECT ENGINEER

This research was supported by the Advanced Research Projects Agency of the Department of Defense and was monitored by Robert W. Hermes under Contract No. DAAK02-72-C-0422.

Contract No. DAAK02-72-C-0422 Effective Date 20 April 1972
Amount of Contract $29,296 Expiration Date 20 Nov 1972

DEVELOPMENT OF VARIABLE AFFINITY BARRIER PHOTOEMITTER

SPONSORED BY:

ADVANCED RESEARCH PROJECTS AGENCY
ARPA ORDER No. 2167

FINAL TECHNICAL REPORT

PREPARED BY:

BETA INDUSTRIES, INC.
DAYTON, OHIO 45429

JOHN L. MIZE
PRINCIPAL INVESTIGATOR & PROJECT ENGINEER

This research was supported by the Advanced Research Projects Agency of the Department of Defense and was monitored by Robert W. Hermes under Contract No. DAAK02-72-C-0422.

FOREWORD

The work discussed in this final report was performed under Contract No. DAAK02-72-C-0422 at Beta Industries, Inc., Dayton, Ohio and Battelle Columbus Laboratories, Columbus, Ohio. The results are being reported according to the requirements of the contract.

The work was conducted during the period from April 1972 through December 1972. The principal investigators were Mr. J. L. Mize for Beta Industries, Inc. and Mr. R. Baxter for Battelle Columbus Laboratories. The contract monitor is Mr. Robert W. Hermes.

BLANK PAGES
IN THIS
DOCUMENT
WERE NOT
FILMED

ABSTRACT

Cold cathode emission was obtained for devices fabricated using Si - SnO_2 heterojunctions. Due to excessive heating the devices failed before photo measurements could be made.

Devices fabricated by "etching" silicon either single crystal or expitaxial exhibited no electron emission.

TABLE OF CONTENTS

LIST OF ILLUSTRATIONS

LIST OF SYMBOLS

I = Variation parameter

j_r = Electron Current density, junction region

j_p = Hole current density, junction region

ε = Electric field, junction region

$\delta_1(0)$ = Voltage drop across the junction

Δ_1 = A constant, heterojunction stop

j_{nr} = Electron current density, radial component, junction region

j_{er} = Emission current density, radial component

$j_{e\theta}$ = Emission current density, angular component

$j_{n\theta}$ = Electron current density, angular component, junction region

$$\delta(r) = \begin{cases} 1 \text{ if } r = 0 \\ 0 \text{ if } r > 0 \end{cases}$$

$$\delta(\theta) = \begin{cases} 1 \text{ if } \theta = 0 \text{ or } \theta = \pi \\ 0 \text{ if } 0 < \theta < \pi \end{cases}$$

j_{pr} = Hole current density, radial component, junction region

$j_{p\theta}$ = Hole current density, angular component, junction region

q = Electron charge

n = Electron concentration, junction region

n_o = Electron concentration at zero electric field, junction region

p = Hole concentration, junction region

p_o = Hole concentration at zero electric field, junction region

J = Variational parameter

$\bar{\varepsilon}_x$ = Electric field, x component, body region

$\bar{a}_y$ = Electric field, y component, body region

$\bar{j}_{nx}$ = Electric current density, x component, body region

$\bar{j}_{ny}$ = Electron current density, y component, body region

$\bar{j}_{px}$ = Hole current density, x component, body region

$\bar{j}_{py}$ = Hole current density, y component, body region

$\bar{n}$ = Electron concentration, body region

$\bar{n}_o$ = Electron concentration, zero electric field, body region

p = Hole concentration, body region

p_o = Hole concentration, zero electric field, body region

G, G_0, G_1 = Variational parameter, body region

$\tilde{j}_{nx}$ = Electron current density, x component, adjacent the junction

$\tilde{j}_{ny}$ = Electron current density, y component, adjacent the junction

$\tilde{j}_{px}$ = Hole current density, x component, adjacent the junction

$\tilde{j}_{py}$ = Hole current density, y component, adjacent the junction

j_{nex} = Electron injection current density, x component

j_{ney} = Electron injection current density, y component

j_{pex} = Hole injection current density, x component

j_{pey} = Hole injection current density, y component

$\bar{F}_{nx}$ = Electron current injection, low, thermal, tunneling, etc., x component

$\bar{F}_{ny}$ = Electron current injection, low, thermal, tunneling, etc., y component

$\bar{F}_{px}$ = Hole current injection, low, thermal, tunneling, etc., x component

$\bar{F}_{py}$ = Hole current injection, low, thermal, tunneling, etc., y component

$$\delta(x,y) = \begin{cases} 0 \text{ if } x,y \text{ are not on the junction} \\ 1 \text{ if } x,y \text{ are on the junction} \end{cases}$$

V_2 = Voltage at x,y

V_{20} = Voltage at $x = L_0$, y

μ_n = Electron mobility

μ_p = Hole mobility

D_n = Electron diffusion constant

D_p = Hole diffusion constant

CHAPTER 1

INTRODUCTION

This research program had as contract goals the fabrication of photo sensitive VAB structures. Unfortunately, due primarily to the initial decision to use thermally grown SiO_2 as the mask, usable structures could not be fabricated. The time wise short program prevented subsequent fabrication based on techniques that would have a greater probability of success.

Some significant advancements in the development of a cogent theory of operation were made. Overall, it must be concluded that this research effort fell short of the goals; however, it must not be concluded that photo sensitive VAB structures are not possible.

CHAPTER 2

PROGRAM SUMMARY

This research and development program was directed toward establishing the feasibility of fabricating high quantum efficiency photo emitters based on the Variable Affinity Barrier.

Although extreme fabrication difficulties were encountered, which necessitated radical changes in emitter designs, a few samples did exhibit electron emission. However, these samples were short lived and photo emissive measurements could not be conducted.

In all, three different design approaches were investigated. These were:

1. Fabricating VAB junctions using single crystal p type silicon.

2. Fabricating VAB junctions using epitaxial p on p+ silicon.

3. Fabricating VAB junctions using a tin oxide film on p type silicon.

Only the last approach was partially successful--emission occurred. However, our results do not preclude that the other two design approaches are unfeasible, but only that during this program it was not possible to fabricate the necessary geometries or heterojunctions.

2.1 Program Implementation

The objective of this R & D effort was to establish the feasibility of using the Variable Affinity Barrier structure--a demonstrated highly efficient cold cathode--as a photo emissive device.

As discussed in some detail in Chapter 3, the necessary conditions for Variable Affinity Barrier is (1) to form a junction, preferably a heterojunction, in the

surface of a semiconductor, (2) the junction interface must substantially be neither parallel nor perpendicular to the surface of the device. This curvilinear geometry (see figure 1) will necessarily create a field internal to the junction region with a component directed toward the surface. Therefore, the design objective of this program was to fabricate devices, generally as shown in figure 1-a.

Based on the phenomenological VAB model, discussed in Chapter 3, it is desirable, but not necessary, that the junction width, 1, be small, say one or two micrometers. Further, the base region thickness, t, should also be small.

In discussion with Battelle Columbus Laboratories, the following fabrication restrictions were imposed:

1. The junction cross section would necessarily be trapezoidal rather than semicircular (see figure 1-b).

2. The junction width, 1, could not be less than five micrometers nor would it be larger than 25 micrometers.

3. The web thickness, t, must be equal to the wafer thickness, T, minus the junction width, 1.

The restrictions were imposed due primarily to equipment limitations at both Beta and Battelle.

Battelle was placed under contract to fabricate devices using p+ silicon wafers supplied by Night Vision Laboratory based on the configuration shown in figure 1-b. Since the Battelle Final Report is addended to this report only the highlights of their effort will be included in the body of this Final Report.

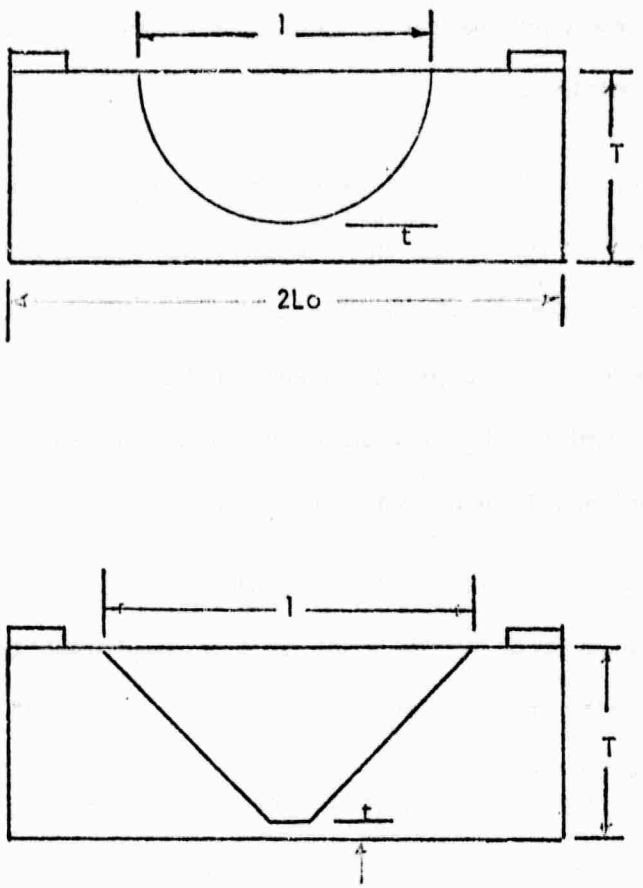

Figure 1. VAB GEOMETRY

At the onset of the fabrication phase of this program difficulties were encountered; it was not possible to etch the wafers without creating a profusion of etch pits. It was established during September 1972 that the NVL supplied silicon wafers could not be etched using the E gas etchant; other silicon wafers could be etched.

Battelle was only partially successful; the new silicon wafers could be etched without introducing etch pits, but the desired geometry could not be achieved. More importantly, however, the heterojunction necessary for a VAB structure could not be formed. These problems were a direct consequence of the decision to use thermally grown SiO_2 as a mask during the etching process. The etch rates of SiO_2 and Si along with the limited thickness of thermally grown SiO_2 prevented Battelle from fabricating useful devices. It must, therefore, be concluded that this phase of the program was completely unsuccessful. Much was learned, but the results were null.

As noted earlier, Beta independently initiated a program to fabricate photo emitters based on fabricating a Si - SnO_2 surface heterojunction and then forming a normal cold cathode in the thin SnO_2 layer (see figure 2). Some success was achieved--emission occurred. However, the devices were short lived and quantitative measurements could not be conducted. This effort will be discussed in Chapter 3. In summary, it must be concluded that this program was not successful in achieving the contract goals, but it should not be concluded that a VAB structure achieving or surpassing the design goals cannot be constructed.

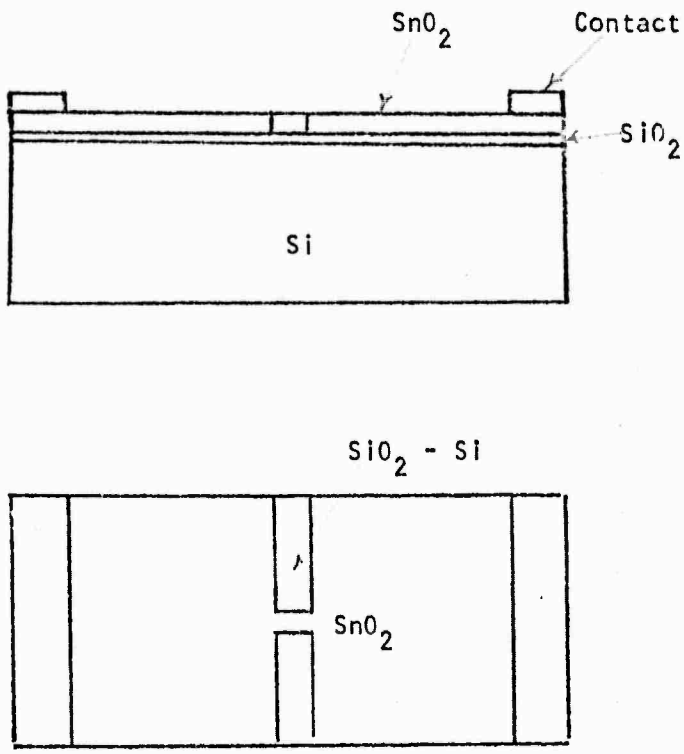

Figure 2. Si-SnO_2 HETEROJUNCTION

CHAPTER 3

PROGRAM PROGRESS REPORT

This research program was planned and implemented to quickly and inexpensively establish the feasibility of the VAB structure as a new type of photo emitter.

Beta, due to the paucity of sophisticated laboratory facilities and expertise in silicon technology, elected to subcontract the fabrication phase of the program; Battelle Columbus Laboratories was selected. This selection was based on:

1. Georgraphical location, Columbus, Ohio,
2. Exceptional laboratory facilities, and
3. General excellence in experimental research.

The Battelle effort is reported in their Final Report addended to this report and will not be discussed in this section.

Beta planned to conduct both theoretical and experimental programs that, in conjunction with the Battelle effort, would establish the feasibility of VAB emitter and meet the goals of the contract. Following is a review in some detail of this effort.

3.1 Theoretical Program

The theoretical effort was initially planned to elucidate the underlying mechanisms of the VAB structures, calculate performance parameters, and establish device designs for use by Battelle in fabricating the experimental devices.

3.1.1 VAB Emission Mechanism

The understanding of VAB structure is simple in concept but difficult to formulate mathematically. These difficulties are due primarily to nonlinearities and lack of definable boundary conditions; in fact, the calculation of boundary conditions at the interface constitutes the major mathematical problem. Both the concept, that is a phenomenological model, and the necessary mathematics are reviewed.

3.1.1.1 Variable Affinity Barrier

To develop a defensible model of any unknown phenomena it is important to review all experimental results such that they can be included or explained by the model. Therefore, the tin oxide Variable Affinity Barrier cold cathode is reviewed prior to formulating a model for a generic VAB structure.

3.1.1.1.1 Tin Oxide Cold Cathode--A Review

Variable Affinity Barriers are usually fabricated by depositing a thin (.01 to 1μm) film of tin oxide on a suitable substrate such as quartz. After metalizing for electrical contacts, the specimen is placed in a vacuum ($\sim 10^{-5}$ torr). When a voltage is applied, heating occurs with the maximum temperature occurring in the necked down region (see figure 3).

When a temperature of approximately 600°C is reached, outgassing occurs and there is an irreversible change in the tin oxide film; electron emission into the vacuum is also observed. In addition, the resistance of the film has increased, usually about 100 times the initial resistance.

Prior to forming the barrier, a scintillating, essentially white light is observed. Figures 4, 5, 6 and 7 illustrate this forming process. On the first

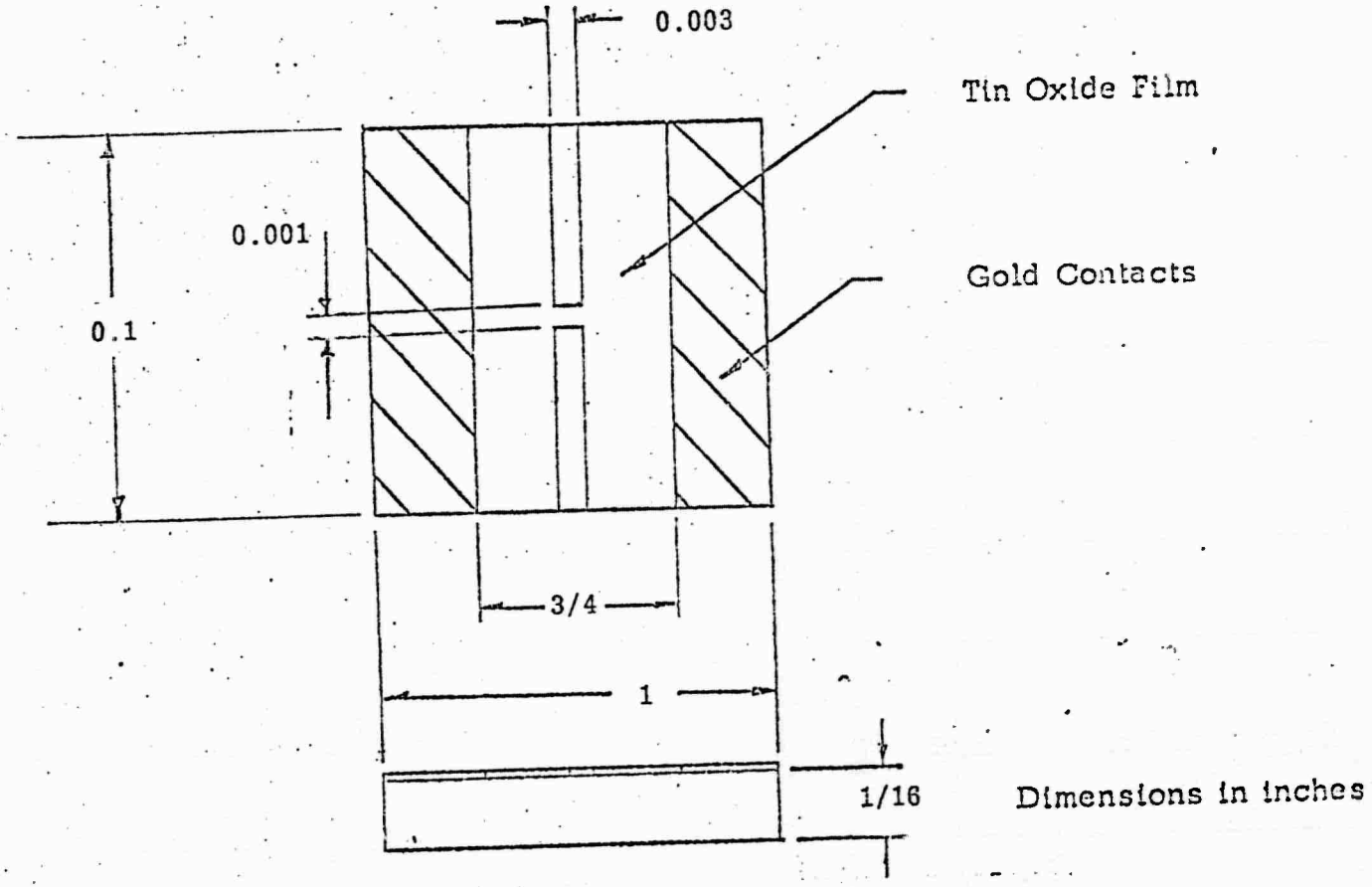

Figure 3. Cathode Design

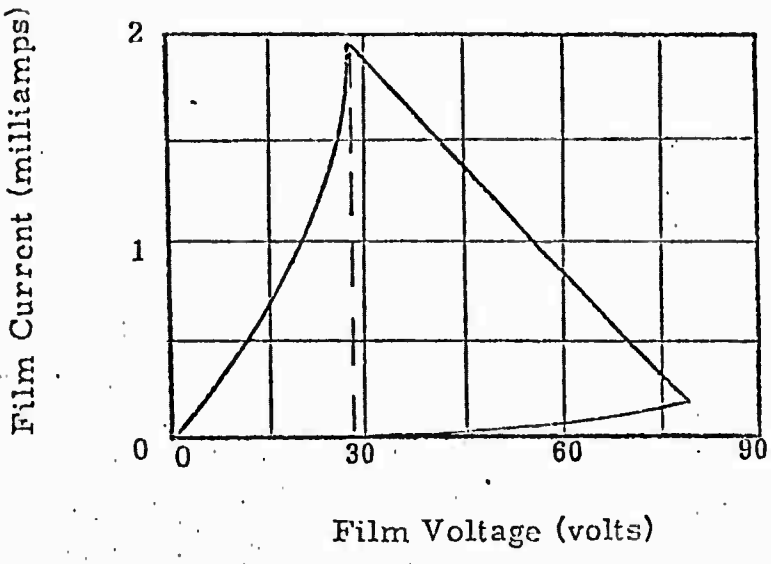

Figure 4. Formation, Film Voltage and Film Current

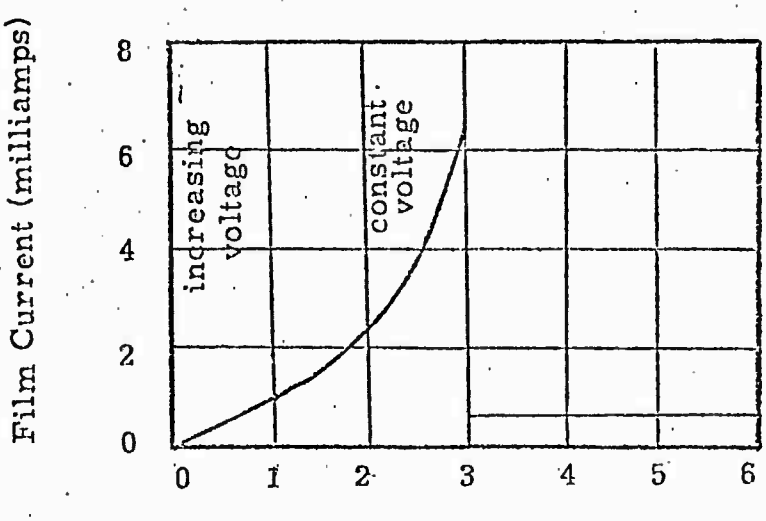

Figure 5. AC Bias - Film Current and Time

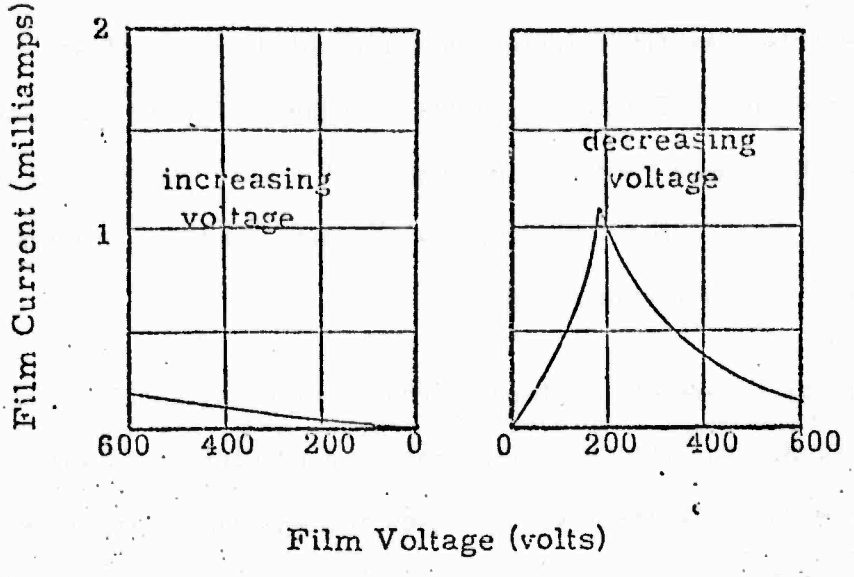

Figure 6. Film Voltage and Film Current

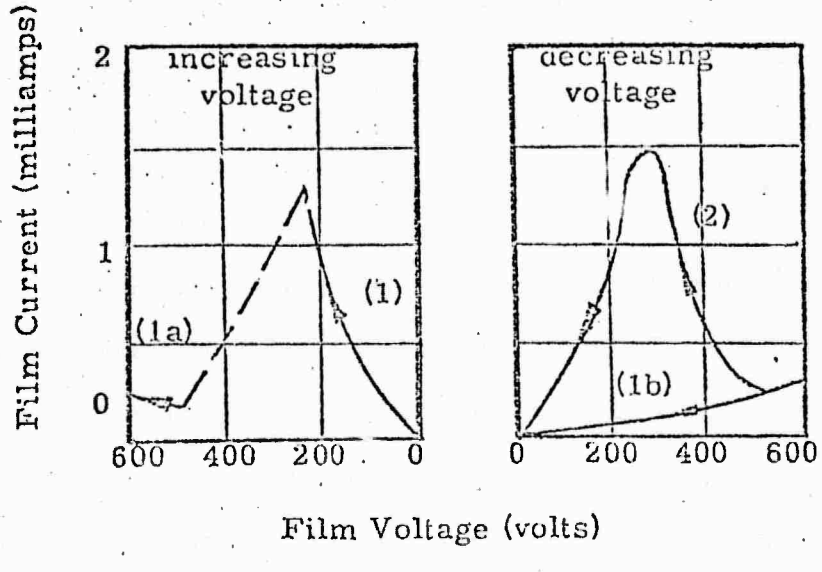

Figure 7. Film Voltage and Film Current

run, figure 4 for a virgin sample, the film current increases greater than linearly until an activation threshold is reached (approximately 30 V) or until the necked down region of the film is heated to approxmately 600°C. At this time, the film resistance increases. The solid curve illustrates the experimental case where, due to the finite impedance of the power supply, the voltage across the sample more than doubled. If a zero impedance source had been used, the voltage across the sample would have remained constant as illustrated by the dashed vertical line.

Figure 5 illustrates some of the time dependent effects associated with the junction formation. For the case illustrated, a 60 hertz bias voltage was applied to the sample. Initially, this bias voltage was increased and the film current increased greater than linearly. When a voltage of approximately 30 volts, rms, was reached, the film current spontaneously increased without increasing the voltage. When the current reached 7.0 milliamps, rms, or at approximately 1.5 watts, the current peaked and then decreased to the high film resistance value of 0.07 milliamps, rms. It should be noted that resistance change (increase) is strongly affected by the contacts and electrical connections. However, in general, the resistance change is proportional to the power dissipated.

Once the formation process is completed a new nonlinearity exists. This is illustrated in figure 6. It is obvious the up trace (increasing voltage) is essentially the same as the high resistance trace in figure 4; however, the down trace exhibits a wild "hysteresis like" effect. The effect, neglecting possible thermal lags, is not hysteresis. In fact, as shown in figure 7, those devices exhibit both switching and memory similar to that exhibited by

some of the chalcogenide glass, amorphous semiconductors and metal oxides. Consider first the switching phenomenon. If the device is initially in its low resistance state, curve 1, and the bias voltage is increased until it exceeds the threshold, in this case 200 volts, the device spontaneously switches to its high resistance state--dashed line. The emitter will remain in the high resistance state for both increasing and decreasing bias voltage, curves 1-a and 1-b. If the emitter is in the high resistance state and the bias voltage is slowly reduced, the emitter will convert to its low resistance state. It will remain in this state for both increasing and decreasing voltage (curves 1 and 2), provided, of course, that the threshold is not again exceeded. In fact, it is possible to cycle more or less at will from one state to the other.

In addition, as illustrated in figure 8, these emitters exhibit a partial memory effect. If the emitter is operating at some point on the negative resistance characteristic, say point B, C or D, the bias voltage is suddenly switched off, then upon reapplication of a bias voltage, the low resistance characteristic OA is not reproduced. Instead, a characteristic OB', OC' or OD' is reproduced depending upon the operating characteristic prior to removing the bias voltage. If the bias voltage exceeds a voltage denoted by V_s, then the film reverts to a lower resistance state. The region enclosed by the characteristic O-D'-A is stable; also, the characteristic A-B-C-D-E is stable. The area enclosed by the characteristics A-B-C-D-D'-C'-B' is unstable and the film will spontaneously revert to the stable terminus, the characteristic A-B-C-D.

A defensible model for the tin oxide structures must explain a number of distinct conduction and emission phenomena, namely:

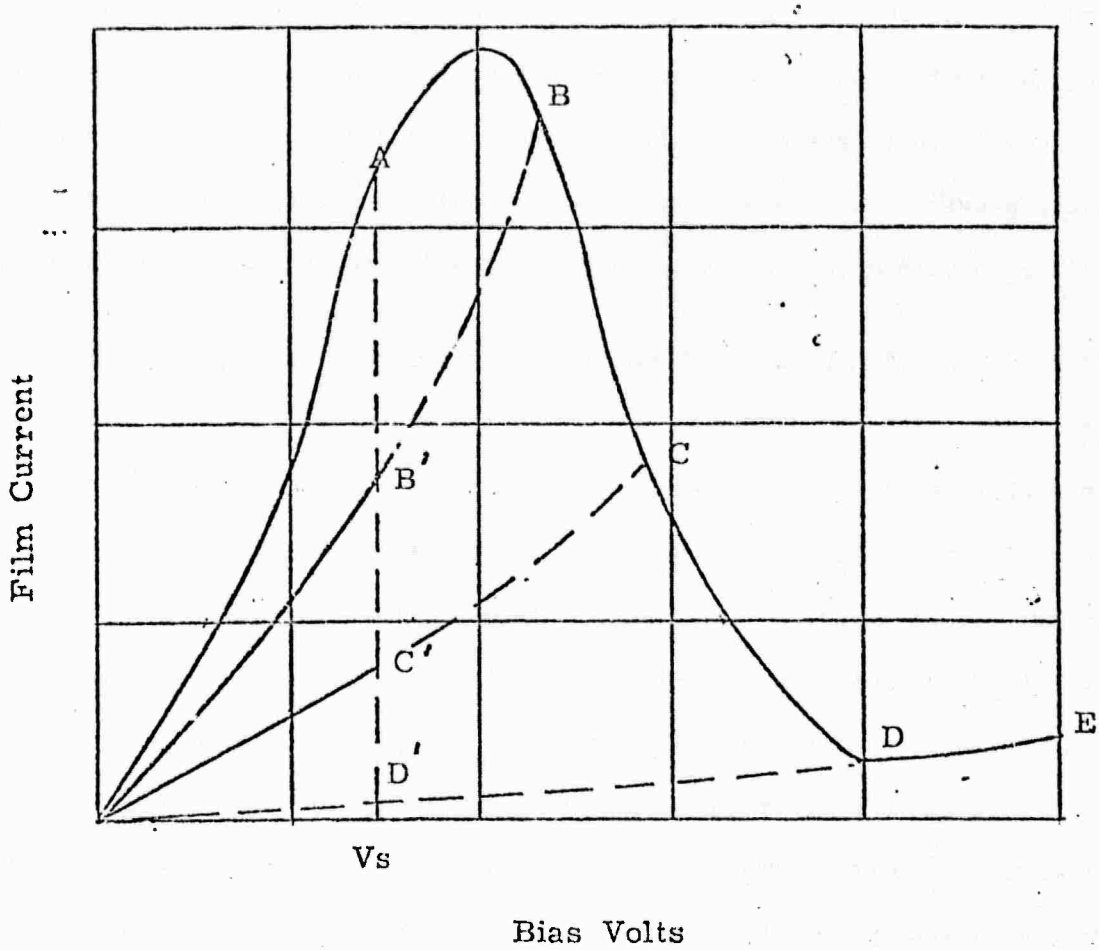

Figure 8.
MEMORY PHENOMENA

1. The onset and increase of conductivity by the application of a voltage prior to activation (i.e., before going high resistance).

2. The formation of the high resistance state by the application of a voltage (i.e., activation).

3. The decrease in conductivity by the application of a voltage (i.e., dynamic negative resistance).

4. The scintillating light, thermal and electroluminescence.

5. The memory and cyclic effect.

6. The high electron transmission coefficient.

The phenomenological model which has been developed is plausible, but incomplete and speculative. It has served and can continue to serve as a framework in which to fit many of the complex experimental observations, to suggest new experimentation and to serve as a guide for improving the VAB cold cathode.

3.1.1.1.2 Variable Affinity Barrier--A Phenomenological Model

The literature is replete with investigations of voltage and current controlled negative resistance in the metal oxide films (2-17). The similarity of results on tin oxide planar structures and those reported on other metal oxide sandwich structures are sufficient to establish that the underlying mechanisms are essentially the same.

However, the different geometries and most importantly the vastly greater electron emission efficiencies are sufficient to require a new model for the devices to be formulated.

Of all the models formulated to explain the onset of conductivity in metal oxide sandwiches, impurity band (hopping) conduction is most plausible. Although the literature (18) does not indicate the existence of traps near the Fermi level in the tin oxide, the probably amorphous nature of the tin oxide films would necessarily indicate that traps would be distributed across the forbidden band, which does support impurity band conduction. The impurity band or traps are most probably due to an oxygen deficiency; of cource, interstitials and other defects would also contribute. Antimony in tin oxide films acts as a reducing agent (14) resulting in donor levels near the bottom of the conduction band.

The variation in resistance as a function of voltage, figure 9, indicates a very low activation voltage which is consistent with the known shallow traps at 0.25 ev (12) below the conduction band.

After the onset of conductivity, many models could be formulated to explain the greater than linear increase of film current with voltage; these include thermal effects, double injection, impurity band conduction, current reduction of the tin oxide, and electro-migration of ions. Again, the phenomena is probably a function of all of these.

Generally, the experimental data favors reduction of the film that is decreased stoichiometry, as the result of electrically heating the film. Of course, this just introduces additional traps or defects throughout the forbidden band which enhances the impurity band conduction.

When the temperature of the film reaches approximately 600°C (1), the film resistance spontaneously increases. At this time or slightly before, a

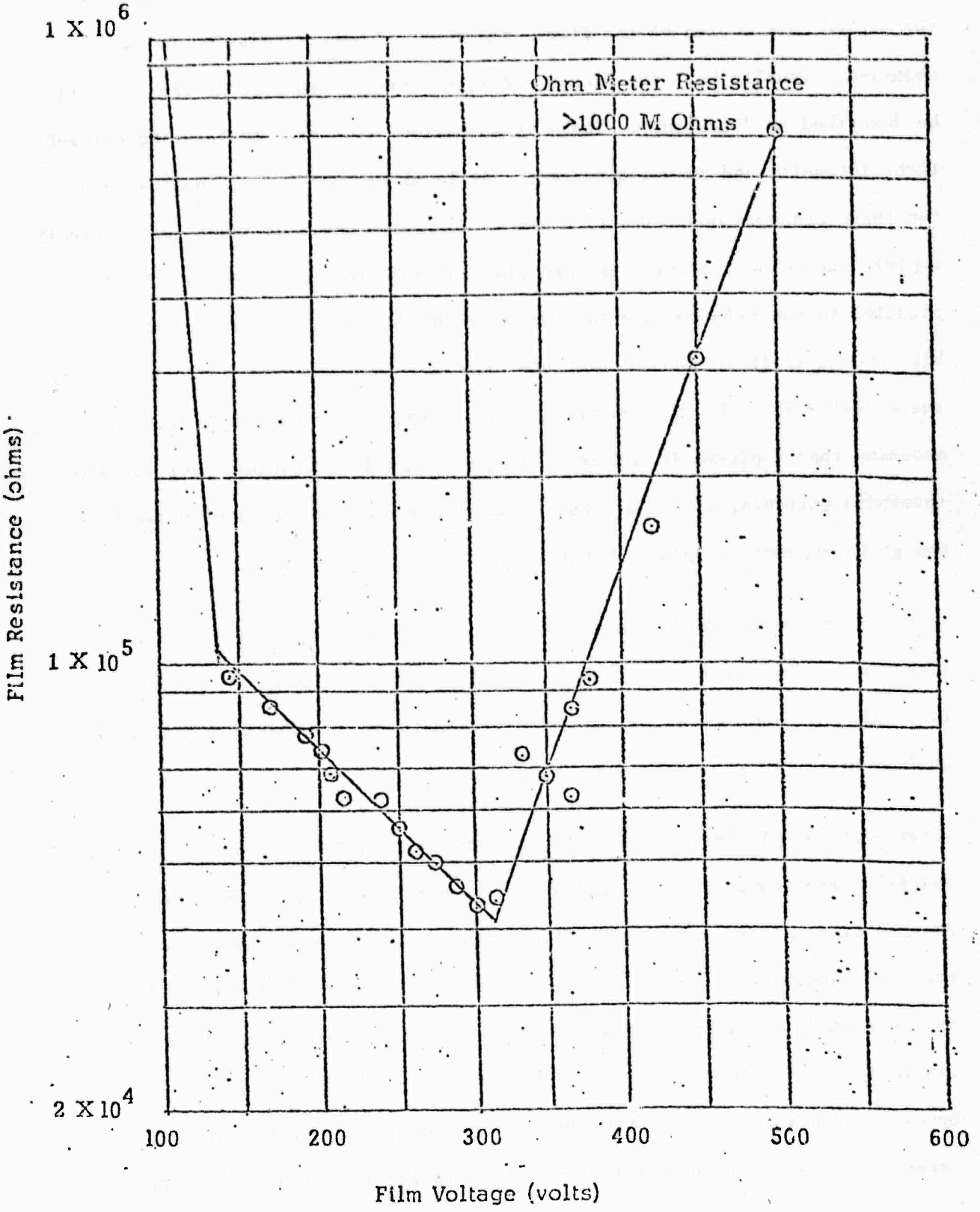

Figure 9. Film Resistance - Film Voltage

scintillating white light appears against a thermal luminescence located in the necked down region of the film. The onset of vacuum emission is also observed. Usually both the vacuum and film currents are erratic and can best be described as "bursting". There is an obvious (visible) correlation between light intensity and emission current. At least two mechanisms could account for these observations. First, a plasma formation could at least qualitatively explain the scintillating light and electron emission; the electric fields parallel to the film surface for the high threshold emitters are centainly high enough if it is assumed that the film is only quasi-continuous. However, the anomalously high emission efficiencies cannot be readily explained by assuming that a plasma is the underlying responsible mechanism. For the low threshold emitters, it is not justifiable to assume that the fields are high enough to support the plasma hypothesis.

A second, and most probably mechanism, is the emission of ions due to the electrical reduction of the film. These ions would not only constitute current carriers, but under the experimental conditions would have a high probability of creating secondaries.

After a period of time, usually one to five minutes, the scintillation and thermal luminescence decrease and a blue electro-luminescence is observed. At this time emission currents tend to stabilize. It is observed that luminescence intensity and emission current are correlated. If the film voltage is now raised, the scintillation returns but again slowly disappears, and stable operation returns. If the film voltage is cycled, the device tends to become more stable; and the frequency of the scintillation occurrence decreases. It has been observed that when operating in a high voltage mode

(~ 100 V) and the film voltage is suddenly reversed, there is an immediate increase in the scintillation and emission current. This supports the hypothesis of ion migration as a contributing factor in the operation of these emitters.

It should be noted that in the above descriptions, it has been tacitly assumed that after activation the cathode has remained in the high resistance state, that it is the O-D-E characteristic of figure 8.

Based on these observations, it is postulated that the activation or forming process is the electrical reduction of the SnO_2 film as illustrated in figure 10. As shown, it has been assumed that the tin dioxide is reduced to tin monoxide in the junction region B; the conditions necessary to explain the observed phenomena are:

1. The junction interface, j, over a substantial portion of its length must be neither perpendicular nor parallel to the emission surface, A.

2. The junction formed must be essentially symmetrical; otherwise, the electrical characteristics will vary with film voltage polarity.

3. The junction must, in the limit of low fields, be high resistance to account for the 100 fold increase in film resistance. The heterojunction, figure 10, would exhibit overall high resistance between the contacts. However, it is unlikely that SnO (a narrow band semiconductor) could support the internal field required for the high emission probability. From reference 28 it can be postulated that the SnO region is completely depleted of charge carriers and is, therefore, an insulating region.

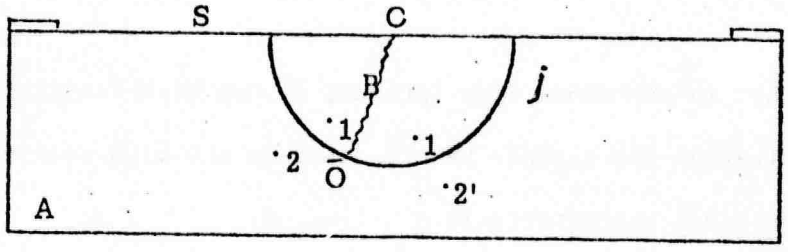

(a)

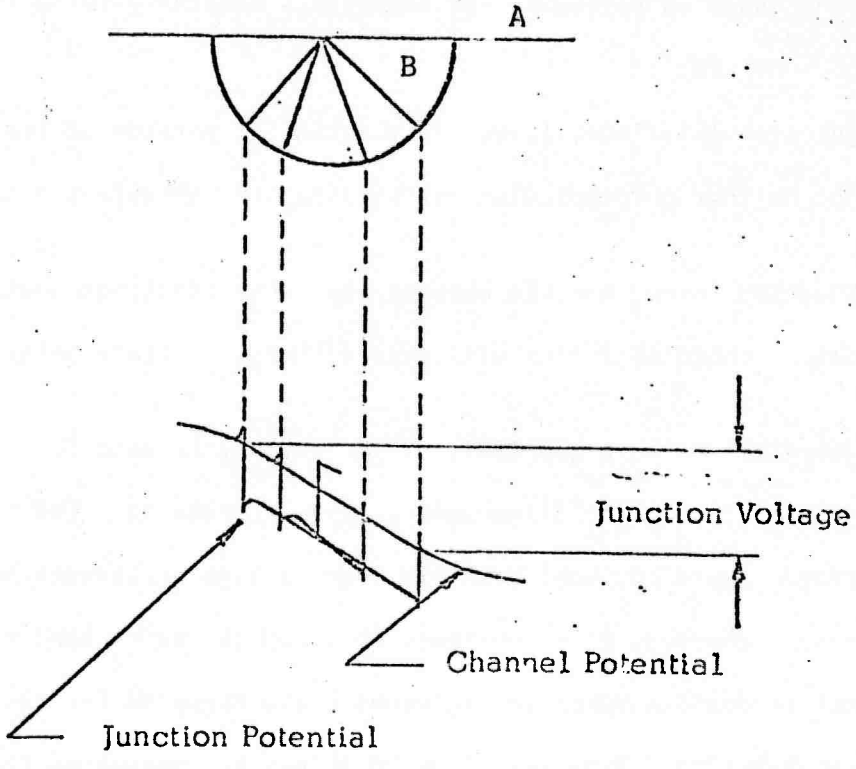

(b)

Figure 10. Cathode Configuration

If these three crucial conditions are met and the dielectric strength (29) of the film is sufficient to support the electric field necessary for emission, the high efficiency cold cathode will result.

The blue luminescence is undoubtedly a radiative recombination process in the junction region of the devices.

This model, at least qualitatively, accounts for all of the phenomena observed when the device is operating in the high resistance state; however, it does not account for the low resistance and negative resistance phenomena. The low resistance leg of the I-V characteristic is similar to the current controlled negative resistance discussed by, among others, Chopra (5), the switching phenomena in amorphous semi-conductors (6, 7 and 8) and the previously mentioned work of Simmons (2 and 3).

It is not clear at this time which mechanism is responsible for the switching and memory observed in the tin oxide films. Arguments can be advanced supporting each of the theories developed to explain the switching and negative resistance phenomena. The partial memory effect, following Simmons (1 and 2), suggests that ion migration and trapped charges are the underlying mechanisms.

The most important characteristics of VAB structures is the curvilinear junction and the existence of a conduction path around the junction (see figure 10). As a consequence, it can be argued that a voltage drop internal to the junction region exist if the potential at the surface is to be single valued--a necessary condition. Following is a review of the mathematical formalism.

3.1.2 Mathematical Formalism--VAB Structure

The phenomenological model previously described is very complicated mathematically. Some of the complications are introduced by space charge limited current

ion migration and "hopping" conduction; but, the postulated geometry, i.e., a semicylindrical heterojunction imbedded in the surface of a wide band gap semiconductor, is of most fundamental importance and also is the most difficult problem to analyze.

At the onset of this theoretical investigation it was decided to ignore or better yet, to assume that the conduction would consist only of drift and diffusion currents. Within this restriction the basic theoretical problem is to determine the two dimensional current flow in the semicylindrical junction region (region B of figure 9-a). If the boundary conditions at the interface, j, and the surface, s, were known then the mathematical development would be straight forward, albiet computationally complicated. However, since these boundary conditions are not known it is necessary to formulate a methodology whereby these boundary conditions can be determined. In fact, once the boundary conditions, particularly the boundary conditions at the surfaces, are known the underlying emission mechanisms will also be known.

It was decided that a variational analysis, i.e., the minimization of the power dissipated, would be sufficient to determine both the current flows and the boundary conditions. It was also decided to introduce as few approximations as possible in formulating the initial, or formal, development and as dictated by computational complexity, to then introduce simplifying assumptions.

Referring to figure 9, it is obvious that it is necessary to develop equations for both the semicylindrical junction region, B, and the body of the device, A, and then to require continuous solutions at the interface, j. This requirement couples the two regions and will, in effect, establish the boundary

conditions at the interface, j. Initially, however, the analysis will proceed as if the regions are uncoupled.

3.1.2.1 Semicylindrical Junction Region

In the junction region (see figure 10) it is convenient to use cyclindrical coordinates and also to separate the problem into two parts--that is, region 1 is by definition that part of the junction that is forward biased and region 2 is the reversed biased portion of the junction.

By definition, the interface between these two regions is the line $0\text{-}\overline{0}$ of figure 10. It is, of course, necessary to require continuity at this interface. For notational simplicity in the forward biased region parameters will be unprimed while in the reversed biased region parameters will be primed. The formal problem is to find the extremum value of J defined by the following integrals:

$$J = \int_{r_o}^{o} \int_{o}^{\theta'} r\,dr\,d\theta \left\{ \left[i_n + j_p \right] \cdot \mathcal{E} + \left| \text{constraints} \right| \right\} \tag{1}$$

$$+ \int_{o}^{r_o} \int_{\theta}^{\pi} r\,dr\,d\theta \left\{ \left[j'_n + j'_p \right] \cdot \mathcal{E} + \left| \text{constraints} \right| \right\}$$

where the usual notation for current densities and electric fields have been employed. The difficulty here is in selecting constraints which do not introduce non-physical solutions.

3.1.2.1.1 Determination of Constraints

It is obvious that the integral of the radial field, εr, from point 1 to point 1' where these points lie wholly within the junction region (figure 10) to a large extent will be determined by the current flow in the body of the device A. Let the voltage between 2 and 2' (located wholly within the body of the device) be denoted by V_1; further, let the voltage between 0 and $\overline{0}$ be denoted by Δ_1, a constant, therefore a necessary constraint is:

$$\delta_1(\theta) = \int_{r_0}^{0} \varepsilon r dr - \left[V_1(\theta) + \Delta_1 \right] \tag{2}$$

where $\delta_1(\theta)$ is the voltage drop across the junction. Similarly for the reversed bias region

$$\delta_1'(\theta) = \int_{0}^{r_0} \varepsilon r dr - \left[V_1'(\theta) - \Delta_1 \right] \tag{3}$$

Other needed auxillary equations are:

$$\int_{0}^{\theta} r \varepsilon_\theta(r) d_\theta = \int_{r}^{0} \varepsilon r(\theta) dr \tag{4}$$

and

$$\int_{\theta'}^{\pi} r \varepsilon_\theta(r) d\theta = \int_{0}^{r} \varepsilon r(\theta) dr \tag{5}$$

additionally

$$\frac{1}{q} \nabla \cdot j_n = \frac{1}{q} \nabla \cdot j_r \tag{6}$$

$$\frac{1}{q}\nabla\cdot j_n' = \frac{1}{q}\nabla\cdot j_r' \tag{7}$$

where

$$j_n \equiv j_{nr} + j_{er}\delta(r) + j_{e\theta}\delta(\theta) + j_{n\theta} \tag{8}$$

$$j_p \equiv j_{pr} + j_{p\theta} \tag{9}$$

$$j_n' \equiv j_{nr}' + j_{n\theta}' \tag{10}$$

$$j_p' \equiv j_{pr}' + j_{p\theta}' \tag{11}$$

$$j_e \equiv F_3 \tag{12}$$

where the j_e's are emission current densities and the δ's are functions which zero everywhere except at the surface; then they are one.

Other needed auxillary equations are:

$$\epsilon_s \nabla\cdot \mathcal{E} \cong q\left[(n-n_o)-(p-p_o)\right] \tag{13}$$

$$\epsilon_s \nabla\cdot \mathcal{E}' \cong q\left[(n'-n_o')-(p'-p_o')\right] \tag{14}$$

$$j_n = q\mu_n n\mathcal{E} + D_n\nabla n \tag{15}$$

$$j'_n = q\mu'_{n,i}\mathcal{E}' + D'_n \nabla n' \tag{16}$$

$$j_p = q\mu_p p \mathcal{E} - D_p \nabla p \tag{17}$$

$$j'_p = q\mu'_p p' \mathcal{E}' - D'_p \nabla'_p \tag{18}$$

where ε is the permitivity and the other notations are standard.

3.1.2.1.2 Variational Problem

The variational problem is simply to find the extremum value for J and J' defined by the following integrals and then to select boundary conditions that conserve continuity between the primed and unprimed variables.

$$J = \int_{r_o}^{o} \int_{o}^{\theta'} r \Big\{ \left[\left(j_{nr} + j_{pr} \right) \mathcal{E}_r + \left(j_{n\theta} + j_{p\theta} \right) \mathcal{E}_\theta \right] \tag{19}$$

$$+ \left[\left(\lambda_1^2(\theta)\mathcal{E}_r^2 + \lambda_2^2(r)\mathcal{E}_\theta^2 \right)^{\frac{1}{8}} - \left(\lambda_1^2(\theta) + \lambda_2^2(r) \right)^{\frac{1}{8}} F_1 \right]$$

$$+ \lambda_5(r,\theta) \Big[\frac{1}{r} \frac{\partial}{\partial r} r \left(j_{nr} + j_{er}\delta(r) - j_{pr} \right)$$

$$+ \frac{1}{r} \frac{\partial}{\partial \theta} \left(j_{n\theta} + j_{e\theta}\delta(\theta) - j_{p\theta} \right) \Big] \Big]$$

$$+\left[\left(\left(\lambda_4(r,\theta)\, j_{er}\,\delta(r)\right)^2+\left(\lambda_5(r,\theta)\, j_{e\theta}\,\delta(\theta)\right)^2\right)^{\frac{1}{2}}\right.$$

$$\left.-\left(\left(\lambda_4(r,\theta)\, F_4\right)^2+\left(\lambda_8(r,\theta)\,\xi_8\right)^2\right)^{\frac{1}{2}}\right]$$

$$+\lambda_5(r,\theta)\left[\frac{\epsilon_s}{r}\left(\frac{\partial}{\partial r}r\,\xi_r+\frac{\partial}{\partial}^{\circ}\right)-q\left(n-n_o-p+p_o\right)\right]$$

$$+\lambda_6(r,\theta)\left[\left(j_{nr}^2+j_{n\theta}^2\right)^{\frac{1}{2}}-\left(\left(q\mu_n n\,\xi r+D_n\frac{\partial n}{\partial r}\right)^2\right.\right.$$

$$\left.\left.+\left(q\mu_n n\,\xi\theta+\frac{D_o}{r}\,\frac{\partial 1}{\partial 0}\right)^2\right)^{\frac{1}{2}}\right]$$

$$+\lambda_7(r,\theta)\left[\left(j_{pr}^2+j_{p\theta}^2\right)^{\frac{1}{2}}-\left(\left(q\mu_p p\,\xi r-D_p\frac{\partial p}{\partial r}\right)^2\right.\right.$$

$$\left.\left.\left.+\left(q\mu_p p\,\xi\theta-\frac{D_p}{r}\,\frac{\partial p}{\partial\theta}\right)^2\right)^{\frac{1}{2}}\right]\right\}dr\,d\theta$$

where

$$F_1 \equiv V_1(\theta)+\Delta_1+\delta_1(\theta) \tag{20}$$

and for the primed system, J' is given by

$$J' = \int_0^{r_0} \int_{\theta'}^{\pi} \Bigg\{ \Big[\Big(j'_{nr} + j'_{pr} \Big) \xi'_r + \Big(j_{n\theta} + j_{p\theta} \Big) \xi'_\theta \Big] \tag{21}$$

$$+ \Big[\Big(\lambda_1^{\prime 2}(\theta) \xi_r^{\prime 2} + \lambda_2^{\prime 2}(r) \xi_\theta^{\prime 2} \Big)^{\frac{1}{2}} - F_1' \Big(\lambda_1^{\prime 2}(\theta) + \lambda_2^{\prime 2}(r) \Big)^{\frac{1}{2}} \Big]$$

$$+ \frac{\lambda'_3(r,\theta)}{r} \Big[\frac{\partial}{\partial r} r \Big(j'_{nr} - j'_{pr} \Big) + \frac{\partial}{\partial \theta} \Big(j'_{n\theta} - j'_{p\theta} \Big) \Big]$$

$$+ \lambda'_5(r,\theta) \Big[\frac{\epsilon_5}{r} \Big(\frac{\partial}{\partial r} r \xi'_r + \frac{\partial}{\partial \theta} \xi'_\theta \Big) - q \Big(n' - n'_0 - p' - p'_0 \Big) \Big]$$

$$+ \lambda_6(r,\theta) \Big[\Big(j_{nr}^{\prime 2} + j_{n\theta}^{\prime 2} \Big)^{\frac{1}{2}} - \Big(\Big| q \mu'_n n' \xi'_r + D'_n \frac{\partial p'}{\partial r} \Big|^2$$

$$+ \Big| q \mu'_p p' \xi'_\theta + \frac{D'_n}{r} \frac{\partial n}{\partial \theta} \Big|^2 \Big)^{\frac{1}{2}} \Big]$$

$$+ \lambda'_7(r,\theta) \Big[\Big(j_{pr}^{\prime 2} + j_{p\theta}^{\prime 2} \Big)^{\frac{1}{2}} - \Big(\Big| q \mu'_p p' \xi'_p - D'_p \frac{\partial p'}{\partial r} \Big|^2$$

$$+ \Big| q \mu'_p p' \xi'_\theta - \frac{D'_p}{r} \frac{\partial p'}{\partial \theta} \Big|^2 \Big)^{\frac{1}{2}} \Big] \Bigg\} dr\, d\theta$$

where

$$F_l' \equiv V_l'(\theta) + \Delta_1 + \delta_l'(\theta) \tag{22}$$

If the integrands of these integrals are denoted by g and g' respectively then for an extremum value the integrands must satisfy the following Euler

$$\frac{\partial g}{\partial E_r} - \frac{\partial}{\partial \theta}\left(\frac{\partial g}{\partial\left(\frac{\partial E_\theta}{\partial \theta}\right)}\right) = 0 \tag{23}$$

$$\frac{\partial g}{\partial E_\theta} - \frac{\partial}{\partial \theta}\left(\frac{\partial g}{\partial\left(\frac{\partial E_\theta}{\partial \theta}\right)}\right) = 0 \tag{24}$$

$$\frac{\partial g}{\partial j_{nr}} - \frac{\partial}{\partial r}\left(\frac{\partial g}{\partial\left(\frac{\partial j_{nr}}{\partial r}\right)}\right) = 0 \tag{25}$$

$$\frac{\partial g}{\partial j_{pr}} - \frac{\partial}{\partial r}\left(\frac{\partial g}{\partial\left(\frac{\partial j_{pr}}{\partial r}\right)}\right) = 0 \tag{26}$$

$$\frac{\partial g}{\partial j_{n\theta}} - \frac{\partial}{\partial \theta}\left(\frac{\partial g}{\partial\left(\frac{\partial j_{n\theta}}{\partial \theta}\right)}\right) = 0 \tag{27}$$

$$\frac{\partial g}{\partial j_{n\theta}} - \frac{\partial}{\partial \theta}\left(\frac{\partial r}{\partial\left(\frac{\partial j_{p\theta}}{\partial \theta}\right)}\right) = 0 \tag{28}$$

$$\frac{\partial g}{\partial n} - \frac{\partial}{\partial r}\left(\frac{\partial g}{\partial\left(\frac{\partial n}{\partial r}\right)}\right) - \frac{\partial}{\partial \theta}\left(\frac{\partial g}{\partial\left(\frac{\partial n}{\partial \theta}\right)}\right) = 0 \tag{29}$$

$$\frac{\partial g}{\partial p} - \frac{\partial}{\partial r}\left(\frac{\partial g}{\partial\left(\frac{\partial p}{\partial r}\right)}\right) - \frac{\partial}{\partial \theta}\left(\frac{\partial g}{\partial\left(\frac{\partial p}{\partial \theta}\right)}\right) = 0 \tag{30}$$

$$\frac{\partial g}{\partial j_{er}} - \frac{\partial}{\partial r}\left(\frac{\partial g}{\partial\left(\frac{\partial j_{er}}{\partial r}\right)}\right) = 0 \tag{31}$$

$$\frac{\partial g}{\partial j_{e\theta}} - \frac{\partial}{\partial \theta}\left(\frac{\partial g}{\partial\left(\frac{\partial j_{e\theta}}{\partial \theta}\right)}\right) = 0 \tag{32}$$

$$\frac{\partial g}{\partial F_1} = 0 \tag{33}$$

and a similar set of equations exist for the primed system. Specifically calculating the various derivatives the Euler equations are:

$$j_{nr} + j_{pr} + \frac{\lambda_1^2 \varepsilon_r}{\left[\lambda_1^2 \varepsilon_r^2 + \lambda_2^2 \varepsilon^2 \theta\right]^{\frac{1}{2}}} + \frac{\lambda_5 \epsilon_s}{r} \tag{34}$$

$$- \frac{\lambda_6 j_{nr}}{\left[j_{nr}^2 + j_{n\theta}^2\right]^{\frac{1}{2}}} - \frac{\lambda_7 j_{pr}}{\left[j_{pr}^2 + j_{p\theta}^2\right]^{\frac{1}{2}}} - \frac{\lambda_2^2 F_2 \left(\frac{\partial F_2}{\partial \varepsilon_r}\right)}{\left[\lambda_2^2 F_2 + \lambda_8^2 F_8^2\right]^{\frac{1}{2}}}$$

$$- \frac{\partial}{\partial r}\left[\lambda_5 \epsilon_s\right] = 0$$

$$j_{n\theta} + j_{p\theta} + \frac{\lambda_2^2 \varepsilon_\theta}{\left[\lambda_1^2 \varepsilon_r^2 + \lambda_2^2 \varepsilon_\theta^2\right]^{\frac{1}{2}}} - \frac{\lambda_6 j_{n\theta}}{\left[j_{nr}^2 + j_{n\theta}^2\right]^{\frac{1}{2}}} \tag{35}$$

$$-\frac{\lambda_7 j_{p\theta}}{\left[j_{pr}^2+j_{p\theta}^2\right]^{\frac{1}{2}}}-\frac{\lambda_8^2 F_8\left|\frac{\partial F_8}{\partial \xi_\theta}\right|}{\left[\lambda_6^2 F_2^2+\lambda_8^2 F_8^2\right]^{\frac{1}{2}}}$$

$$-\frac{\partial}{\partial\theta}\left[\frac{\lambda_5 \epsilon_s}{r}\right]=0$$

$$\xi_r+\frac{\lambda_3}{r}+\frac{\lambda_6 j_{nr}}{\left[j_{nr}^2+j_{n\theta}^2\right]^{\frac{1}{2}}}-\frac{\partial}{\partial\theta}\lambda=0 \tag{36}$$

$$\xi_\theta+\frac{\lambda_6 j_{n\theta}}{\left[j_{nr}^2+j_{n\theta}^2\right]^{\frac{1}{2}}}-\frac{\partial}{\partial 0}\frac{\lambda_3}{r}=0 \tag{37}$$

$$\xi_r-\frac{\lambda_3}{r}+\frac{\lambda_7 j_{pr}}{\left[j_{pr}^2+j_{p\theta}^2\right]^{\frac{1}{2}}}+\frac{\partial}{\partial\theta}\lambda_3=0 \tag{38}$$

$$\xi_\theta+\frac{\lambda_7 j_{p\theta}}{\left[j_{pr}^2+j_{p\theta}^2\right]^{\frac{1}{2}}}+\frac{\partial}{\partial\theta}\frac{\lambda_3}{r}=0 \tag{39}$$

$$-\lambda_5 q-\frac{\lambda_6 q\mu_n\left[\xi_r j_{nr}+\xi_\theta j_{n\theta}\right]}{\left[j_{nr}^2+j_{n\theta}^2\right]} \tag{40}$$

$$+\frac{\partial}{\partial r}\left[\frac{\lambda_6 D_n j_{nr_1}}{\left[j_{nr}^2+j_{n\theta}^2\right]^{\frac{1}{2}}}\right]+\frac{\partial}{\partial\theta}\left[\frac{\lambda_6 D_n j_{n\theta}}{r\left[j_{nr}^2+j_{n\theta}^2\right]^{\frac{1}{2}}}\right]=0$$

$$\lambda_5 q - \frac{\lambda_7 q \mu_{p_r} j_{pr} + \xi_\theta j_{p\theta}}{\left[j_{pr}^2 + j_{p\theta}^2\right]^{\frac{1}{2}}} \tag{41}$$

$$+ \frac{\partial}{\partial r}\left[\frac{\lambda_7 D_p j_{pr}}{\left[j_{pr}^2 + j_{p\theta}^2\right]^{\frac{1}{2}}}\right] + \frac{\partial}{\partial \theta}\left[\frac{\lambda_7 D_p j_{p\theta}}{r\left[j_{pr} + j_{p\theta}\right]^{\frac{1}{2}}}\right] = 0$$

$$\lambda_3 \delta(r) + \frac{\lambda_4 j_{er} \delta^2(\theta)}{\left[\lambda_4^2 j_{er}^2 \delta^2(r) + \lambda_5^2 j_{e\theta} \delta^2(\theta)\right]^{\frac{1}{2}}} - \frac{\partial}{\partial r}\lambda_3 \delta(r) = 0 \tag{42}$$

$$\frac{\lambda_8^2 j_{e\theta} \delta^2(\theta)}{\left[\lambda_4^2 j_{er}^2 \delta^2(r) + \lambda_5^2 j_{e\theta}^2 \delta^2(\theta)\right]^{\frac{1}{2}}} - \frac{\partial}{\partial \theta}\left[\frac{\lambda_3 \delta(\theta)}{r}\right] = 0 \tag{43}$$

$$\lambda_1^2 + \lambda_2^2 = 0 \tag{44}$$

The solution of these simultaneous differential equations along with the equation to include the variable end point, θ', could, in theory, be solved in terms of F_1 and F_2, the junction boundary condition and the emission function. However, it is not possible to include the transversality conditions explicitly. If a function, an unknown function, ψ is defined to describe the loci of constant potential between the origin and the junction, then the transversality conditons are formally:

$$g + \left(\frac{\partial \Psi}{\partial r} - \frac{\partial g}{\partial r}\right) \frac{\partial g}{\partial\left(\frac{\partial r}{\partial g}\right)} = 0 \tag{45}$$

Thus, formally the problem can be solved in terms of three unknown functions, F_1, F_2 and ψ. By including the primed system the dependence on ψ could be

removed. However, before the dependence on F_1 can be removed it is necessary to include the equations governing the current flow in the body of the device.

3.1.2.2 Body Region

In the body region there is no particularly convenient coordinate system; therefore, rectangular coordinates will be used. Again, it is convenient to analyze the problem in two parts, denoted by primed and unprimed variables. As in the previous section the determination of the constraints is most important. Referring to figure 11-a it is obvious that

$$V_2 - \left[\int_0^{L_o - r_o} \bar{\xi}_x \, dx + \int_{L_o - r_o}^{L_o - \sqrt{r^2 - y^2}} \bar{\xi}_x \, dx \right] = 0 \quad \text{if } x > |L_o - r_o| \tag{46}$$

where body parameters are barred.

Following the same rational used in the junction region, the variational problem now becomes find the extremum value of G and G' where G is defined by:

$$G = G_0 + G_1 \tag{47}$$

$$G_0 = \int_0^{L_o - r_o} dx \int_0^{-l_o} dy \left\{ \left[\left| \bar{j}_{nx} + \bar{j}_{px} \right| \xi_x + \left| \bar{j}_{ny} + \bar{j}_{py} \right| \xi_y \right] \right. \tag{48}$$

$$+ \gamma_1 \left[\bar{\epsilon}_s \left| \frac{\partial \bar{\xi}_p}{\partial p} + \frac{\partial \xi_y}{\partial y} \right| - q \left| \bar{n} - \bar{n}_o - \bar{p} + \bar{p}_o \right| \right]$$

$$\left. + \gamma_2 \left[\left| \bar{j}_{nx}^2 + \bar{j}_{ny}^2 \right|^{\frac{1}{2}} - \left| q \bar{\mu}_n \bar{n} \bar{\xi}_x + \bar{D}_n \frac{\partial \bar{n}}{\partial y} \right| \right]^2 \right.$$

$$+ \left| j\bar{\mu}_n \bar{n} \bar{\xi}_y - \bar{D}_n \frac{\partial \bar{n}}{\partial y} \right|^2 \Big|^{\frac{1}{2}} \Big]$$

$$+ \gamma_3 \Big[\Big| \bar{j}_{px}^2 + \bar{j}_{py}^2 \Big|^{\frac{1}{2}} - \Big| \left| q\bar{\mu}_p \bar{p} \bar{\xi}_x - \bar{D}_p \frac{\partial \bar{p}}{\partial x} \right|^2$$

$$+ \left| q\bar{\mu}_p \bar{p} \bar{\xi}_y - \bar{D}_p \frac{\partial \bar{p}}{\partial y} \right|^2 \Big|^{\frac{1}{2}} \Big]$$

$$+ \gamma_4 \Big[\frac{\partial}{\partial x} \left(\bar{j}_{nx} - \bar{j}_{px} \right) + \frac{\partial}{\partial x} \left(\bar{j}_{ny} - \bar{j}_{py} \right) \Big]$$

$$+ \gamma_5 \Big[\frac{V_{2o}}{L_o - r} - \bar{\xi}_x \Big] \Big\}$$

$$G_1 = \int_{L_o - r_o}^{L_o} dx \int_{\sqrt{r_o^2 - (L_o - r)^2}}^{-l_o} dy \Big\{ \Big[\left(\tilde{j}_{nx} - \tilde{j}_{px} \right) \tilde{\xi}_x + \left(\tilde{j}_{ny} - \tilde{j}_{py} \right) \tilde{\xi}_y \Big] \quad (49)$$

$$+ \tilde{\gamma}_1 \Big[\tilde{\epsilon}_s \Big(\frac{\partial \tilde{\xi}_x}{\partial x} + \frac{\partial \tilde{\xi}_y}{\partial y} \Big) - q \left(\tilde{n} - \tilde{n}_o - \tilde{p} + \tilde{p}_o \right) \Big]$$

$$+ \tilde{\gamma}_2 \Big[\Big(\left| \tilde{j}_{nx} - \tilde{j}_{nex} \delta(x,y) \right|^2 + \left| \tilde{j}_{ny} + \tilde{j}_{ney} \delta(x,y) \right|^2 \Big)^{\frac{1}{2}}$$

$$- \Big| \left| q\tilde{\mu}_n \tilde{n} \tilde{\xi}_x + \tilde{F}_{nx}(\tilde{\xi}_x, x, y) \right| + \tilde{D}_o \frac{\partial \tilde{n}}{\partial x} \Big|^2$$

$$+\left|q\tilde{\mu}_n\tilde{n}\tilde{\xi}_y+\tilde{F}_{ny}\left|\tilde{\xi}_y,x,y\right|+\tilde{D}_o\frac{\partial\tilde{n}}{\partial y}\right|^2\Big|^{\frac{1}{2}}\Big]$$

$$+\tilde{\gamma}_3\Big[\Big|\left|\tilde{j}_{px}+\tilde{j}_{pex}\delta(x,y)\right|^2+\left|\tilde{j}_{py}+\tilde{j}_{pey}\delta(x,y)\right|^2\Big|^{\frac{1}{2}}$$

$$-\Big|\left|q\tilde{\mu}_p\tilde{p}\tilde{\xi}x+\tilde{F}_{px}\left|\tilde{\xi}x,x,y\right|-\tilde{D}_p\frac{\partial\tilde{p}}{\partial x}\right|^2$$

$$+\left|q\tilde{\mu}_p\tilde{p}\tilde{\xi}_y+\tilde{F}_{py}\left|\tilde{\xi}_y,x,y\right|-\tilde{D}_p\frac{\partial\tilde{p}}{\partial y}\right|^2\Big|^{\frac{1}{2}}\Big]$$

$$+\tilde{\gamma}_4\Big[\frac{\partial}{\partial x}\left|\tilde{j}_{np}+\tilde{j}_{nex}\delta(x,y)-\tilde{j}_{px}-\tilde{j}_{pex}\delta(x,y)\right|$$

$$+\frac{\partial}{\partial y}\left|\tilde{j}_{ny}+\tilde{j}_{ney}\delta(x,y)-\tilde{j}_{py}-\tilde{j}_{pey}\delta(x,y)\right|\Big]$$

$$+\gamma_5\Big[\Big|\frac{V_2\ V_{2o}}{r_o}\Big|-\mathcal{E}_x\Big]\Big\}$$

$$V_{1o}\equiv\int_0^{L_o-r_o}\tilde{\xi}+dx \tag{50}$$

In a similar manner to that used in the junction region, a set of simultaneous equations (the Euler equations) can be calculated for the body of the devices. By requiring continuity between the primed and unprimed regions as well as across the junction, it is in theory at least possible to completely describe

the VAB device. It is, of course, necessary to assume a form for the emission functions, i.e., F_3, the vacuum emission function and $\overline{F}_{nx}$, $\overline{F}_{ny}$, $\overline{F}_{px}$, $\overline{F}_{py}$, $\overline{F}'_{nx}$, $\overline{F}'_{ny}$, $\overline{F}'_{px}$, and $\overline{F}'_{py}$ the junction emission functions. Standard functions such as thermal emission, hot electron emission, tunneling, etc. should be used for these functions.

In practice, however, these equations have not proven tractable.

Before any meaningful results can be derived from this set of rather formidable equations it is necessary to introduce a number of simplifying assumptions. Most of these simplifications, such as assuming that hole and diffusion currents are negligible, are justifiable; however, even with these simplifications the equations are unsolvable. The most important assumption is that the device can be described in terms of some average value of the current density components, such as $\hat{i}_r$, $\hat{i}x$, etc., where the caret was introduced to indicate some kind of current average. This assumption is tantamount to assuming that the current components are independent. Specializing to the junction region then:

$$d\hat{i}_r = rq\mu\hat{n}\xi_r d\theta \tag{51}$$

$$d\hat{i}_r = rq\mu\hat{n}\xi_\theta dr \tag{52}$$

$$q\bar{n} = \epsilon \frac{1}{r}\frac{d_r\xi_r}{dr} \tag{53}$$

Now in the sense of the averages used in this approximateion $\frac{d\hat{i}_r}{d\theta}$ is a function of r only. Solving equation 51 gives:

$$\xi_r = \frac{1}{r}\sqrt{\left|\frac{d\hat{i}_r}{d}\right|\frac{1}{\mu\epsilon}}\sqrt{r_o^2 - r^2} + \xi_r\left|r = r_o\right. \tag{54}$$

substituting equation 54 into equation 52 results in:

$$\xi_\theta = -\frac{\frac{d\hat{i}_\theta}{dr}\sqrt{r_o^2 - r^2}}{\sqrt{\left|\frac{d\hat{i}_r}{d\theta}\right|\mu\epsilon}} \tag{55}$$

solving equation 54 for the potential gives:

$$V(r,\theta) = V_o - \sqrt{\left|\frac{d\hat{i}_r}{d\theta}\right|\frac{1}{\mu\epsilon}}\left\{\sqrt{r_o^2 - r^2}\right. \tag{56}$$

$$\left. + r_o \ln\left[\frac{r_o + \sqrt{r_o^2 - r^2}}{r_o}\right]\right.$$

$$+ \xi_r(r = r_o)\, r$$

Now we are interested in describing the device in terms of the potential difference $\Delta V_o(\theta)$, thus:

$$\Delta V_o = \sqrt{\frac{d\hat{i}_r}{d\theta}\frac{1}{\mu\epsilon}}\,(1 - \ln 2) + \xi_r(r = r_o)\, r \tag{57}$$

and for the special case $\varepsilon_r(r=ro) = o$, ΔV_o is:

$$\Delta V_o = \sqrt{\left|\frac{d\hat{i}_r}{d\theta}\right|\frac{1}{\mu\epsilon}}\,|1 - \ln 2| \tag{58}$$

solving this equation for $\frac{d\hat{i}_r}{d\theta}$ and substituting into equation 55 gives:

$$\frac{d\hat{i}_r}{d\theta} = -\frac{\Delta V_o(\theta)\mu\epsilon}{|1 - \ln 2|^2} \tag{59}$$

where $\frac{i}{r}\frac{d\Delta V_1}{d\theta} = \varepsilon_\theta$ has been used.

Thus, the current density components internal to the junction region are:

$$\frac{d\Delta V}{d\theta} = -\frac{d\hat{i}\theta}{dr}\frac{\sqrt{r_o^2 - r^2}\,|1 - \ln 2|}{\Delta V} \tag{60}$$

$$\frac{d\hat{i}\theta}{dr} = \left[\frac{d}{d\theta}\Delta V^2\right]\left[\frac{1}{2\sqrt{r_o^2 - r^2}\,|1 - \ln 2|}\right] \tag{61}$$

The problem remaining is to relate the junction current densities $\frac{d\hat{i}r}{d\theta}$ and $\frac{d\hat{i}\theta}{dr}$ with the current flow and the body of the device. If the same spirit of approximation that was used in the junction region is used in the body region then the total body current is:

$$I(x) = q\bar{\mu}\bar{n}\xi x f \tag{62}$$

$$I(x) = I_o - \int_o^x \left[\frac{d\hat{i}r}{d\theta} + \frac{d\hat{i}\theta}{dr}\bigg|_{r=\epsilon'}\right] dx \tag{63}$$

where again the bar represents body parameters. I_o is, of course, the current in the body far removed from the junction region. The integral is the total current injected into the junction over the interval o - x taking the deriva-

$$\frac{d}{dx}\left[q\mu n \xi x f\right] = -\left[\frac{\Delta V_o^2 \mu_. \epsilon}{|1 - \ln 2|^2} + \frac{d}{d\epsilon}|\Delta V_o|^2 C_1\right] \tag{64}$$

where

$$C_1 \cong \frac{4}{|1 - \ln 2|} \tag{65}$$

Equation 54 can be put into the form of a differential equation using either x or θ as the independent variable. However, little success has been achieved in effecting a closed form solution. However, considering the physical situation it is reasonable to postulate that the rate of change the body current with position will be small or:

$$\Delta V_o^2 \cong \Delta V_o^2(\theta=0)\left[e^{-\alpha x} - e^{-\alpha r_o}\right] \tag{66}$$

Using equation 66 and 64 and solving for f gives a decreasing exponential form rather than the postulated semi-circular form. However, the general agreement in form indicates that equation 66 is not too bad of an approximation for ΔV_o.

Other needed equations are:

$$\frac{d\Delta r}{d\theta} \cong \frac{\Delta V_o^2 e^{-\alpha r_o}}{(1-\ln 2)}\left[e^{\alpha r_o \cos\theta} - 1\right] \tag{67}$$

$$\xi_r \cong \frac{\Delta V_o^2 e^{\frac{\alpha r_o}{2}}}{r(1-\ln 2)}\sqrt{e^{\alpha r_o \cos\theta} - 1}\sqrt{r_o^2 - r^2} \tag{68}$$

A general, albiet approximate, closed form solution has been derived. However, it is still necessary to derive an expression for the emission current, Ie.

Preliminary measurements of the distribution of the energy spread is very narrow, less 1.3 ev; therefore, it is reasonable to represent the emission probability function by:

$$P = \begin{cases} 0 & \text{if } \mu\xi_r \sin\theta < V_o \\ 1 & \text{if } \mu\xi_r \sin\theta > V_o \end{cases} \tag{69}$$

$$V_o^2 = \frac{2qV_b}{m^x} \tag{70}$$

where V_b is the vacuum barrier, in volts, and m^x is of course the effective mass of the junction electrons. The emission current can now formally be represented by:

$$Ie \cong \int_{\theta_o}^{\frac{\pi}{2}} d\theta \, \frac{\Delta V_o^2 \left| e^{+dr\cos\theta} - 1 \right| - \alpha r_o e\mu\epsilon}{\left| 1 - \ln 2 \right|^2} \tag{71}$$

where θ_o is an adjustable parameter which determines the dark current, Iedc. However, it is more important to establish a dependency on the applied voltage V_o rather than the voltage across the junction region. This relationship between the applied and the junction voltage is simply:

$$\Delta V_o = \frac{V_o}{1 + 2\alpha L_o \frac{m_o}{n} - \int_{\theta_o}^{\pi} Q \, d\theta} \tag{72}$$

where

$$Q = \frac{\left[e^{-\alpha r_o} \left| e^{\alpha r_o \cos\theta} - 1 \right| \right] \mu\epsilon}{\left| 1 - \ln 2 \right|^2} \tag{73}$$

where n_o is the number of current carriers in the dark and n is the total number of current carriers. L_o is 1/2 the length of the device and α is of the form of $\frac{-1}{r_o}$ in $(\frac{\Delta}{r_o})$; Δ is the web thickness. The photo conductive gain, G, is given by:

$$G = \frac{1}{\tau e}\left[\frac{V_o \alpha \frac{n_o}{n} \mu}{1 + 2\alpha \frac{L_o n_o}{n} - \int_{\theta}^{\frac{\pi}{2}} Q \, d\theta}\right] \tag{74}$$

now $\frac{2\alpha L_o n_o}{n} \gg \left[1 - \int_{\theta_1}^{\pi/2} Q \, d\theta\right]$ therefore, the gain is approximately:

$$G \cong \frac{V_o \mu}{2 \tau e L_o} \tag{75}$$

The photo emissive current is:

$$I_e = I_{eDc}\left[1 + \frac{\Delta n}{n_o} \frac{V_o \mu}{2 \tau e L_o}\right] \tag{76}$$

and

$$I_{eDc} = \int_{\theta}^{\frac{\pi}{2}} d\theta \; \frac{V_o^2 e^{2\alpha r_o} \left| e^{\alpha r_o \cos\theta} - 1 \right| \mu \epsilon}{\left| 1 - \ln 2 \right|^2} \tag{77}$$

It can be seen by examining equations 76 and 77 that the VAB structure has the potential for the development of a very efficient photo emissive device.

3.2 Experimental Program - Beta

The essentially null results of the Battelle effort required that Beta look to other design approaches for the VAB photo cathode. The approach selected by Beta was to fabricate a normal tin oxide cold cathode on the surface of a p+ silicon wafer, essentially as shown in figure 2. The band structure of the

Si - SnO_2 heterojunction essentially will be shown as in figure 11 (reference 30).

The problem is to design a structure such that the dark current flow through the silicon is small and such that a modulation of the current carriers in the silicon will modulate the voltage across the junction region of the tin oxide cold cathode. Further, these should be accomplished without sacrificing the photo conductive gain.

The ideal approach is shown in figure 11. The p++ hole injecting contact allows for adjusting the potential of the silicon wafer relation to the contacts without a concomitant change in the hole current. The silicon relative to the tin oxide will behave as a hole sink. Thus, electrons photo excited in the silicon will diffuse into the tin oxide layer. If the tin oxide layer is of relatively high resistance then the increased carriers (electrons) will modulate the voltage across the junction region. In addition, a form of photo conductive gain will also be present.

Beta, at this juncture, had neither time nor facilities to fabricate this "ideal" device (a lack of diffusion or ion implantation equipment). It was, therefore, decided to fabricate a device without the p++ contact. Two devices were fabricated; both exhibited electron emission. However, the film currents were exceedingly high ($\sim$ 200 ma) and the silicon overheated and the devices were destroyed.

It is believed that the metal contacts diffused through the tin oxide film and made intimate electrical contact with the silicon. The silicon base was therefore subjected to high current densities and excessive ohmic heating.

The samples submitted to Beta by Battelle, not suprisingly, exhibited no emission characteristics.

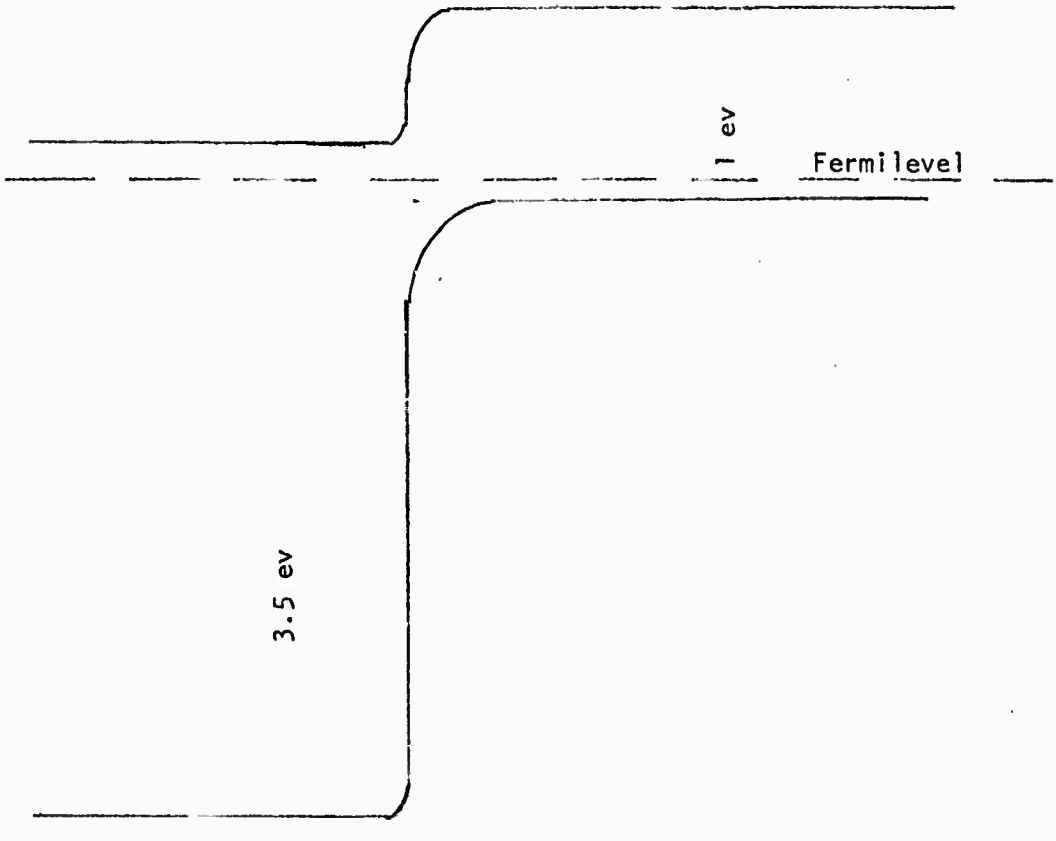

Figure 11. BAND STRUCTU‹E Si - SnO_2 HETEROJUNCTION

THIS
PAGE
IS
MISSING
IN
ORIGINAL
DOCUMENT

CHAPTER 4

CONCLUSIONS AND RECOMMENDATIONS

The experimental results from the research and development fell far short of the contract goals. A number of valid reasons can be advanced, of which, the most important are:

1. The program goals apparently were overly ambitious for the estimated time and monies allocated to the program.

2. Battelle, while generally knowledgeable in silicon technology, did not have specific experience in fabricating these silicon devices. Therefore, when problems arose Battelle could not quickly establish the reasons and effect solutions. Thus, Battelle was unable to deliver any usable devices.

3. The silicon supplied by the Night Vision Laboratory could not be etched without introducing an unacceptable level of etch pits. Too much time was spent trying to use these silicon chips. Thus, very little time could be spent fabricating devices from more acceptable silicon.

4. In retrospect, the inexperience of Beta personnel in the silicon technologies also was a contributing factor. Beta, like Battelle, was unable to quickly establish reasons and effect solutions for the difficulties encountered.

In spite of the lack of experimental success this program did result in a number of positive achievements. These include:

1. A more definitive description of the basic effects of and importance of curvilinear junction devices. In particular, planar structure incorporating curvilinear heterojunction.

2. Basic design concepts for fabricating VAB photo sensitive devices were formulated.

3. Necessary fabrication steps for the VAB devices were established.

Beta strongly believes that steps should be initiated to develop these VAB photo sensitive devices. However, in view of the difficulties encountered in this program any subsequent programs should be based on less ambitious goals and with time to resolve problems which are bound to arise.

REFERENCES

1. Elinson, M. I., Zhdan, A. G., Kudintseva, G. H., Chugunova, M. E., "The Emission of Hot Electrons and the Field Emission of Electrons from the Tin Oxide", Radio Engineering and Electronic Physics, No. 8, Aug 1965, 1290-1296.

2. Simmons, J. G., Verderber, R. R., "New Conduction and Reversible Memory Phenomena in Thin Insulating Film", Proceedings Royal Society, London, 301, 12 April 1967, 77-102.

3. Verderber, R. R., Simmons, J. G., Eales, B., "Forming Process in Evaporated SiO Thin Films", Philisophical Magazine, 1967, 1044-1061.

4. Hickmott, T. W., "Potential Distributions and Negative Resistance in Thin Film Oxide Films", Journal of Applied Physics, Vol 35, No. 9, Sep 1964, 2674-2689.

5. Hickmott, T. W., "Electron Emission, Electroluminescence, and Voltage Controlled Negative Resistance in Al-Al_2O_3-Al Diodes", Journal of Applied Physics, Vol 36, No. 6, June 1965, 1885-1896.

6. Hickmott, T. W., "Impurity Conduction and Negative Resistance in Thin Oxide Films", Journal of Applied Physics, Vol 35, No. 7, July 1964, 2118-2122.

7. Hickmott, J. W., "Low Frequency Negative Resistance in Thin Anodic Oxide Films", Journal of Applied Physics, Vol 33, No. 9, Sep 1962, 2664-2682.

8. Tantraporn, W., "Electron Current Through Metal-Insulator Metal Sandwiches", Solid State Electronics, Pergamon Press, Vol 7, 81-91.

9. Kanter, H., Feibelman, W. A., "Electron Emission from Thin Al-Al_2O_3-Al", Journal of Applied Physics, Vol 33, No. 12, Dec 1961, 3580-3588.

10. Gibbons, J. R., Beadle, U.E., "Switching Properties of Thin NiO Films", Solid State Electronics, Pergamon Press, 1964, Vol 7, 785-797.

11. Toda, M., "A Plasma Instability Induced by Electron-Hole Generation in Impact Ionization", Journal of Applied Physics, Vol 37, No. 1, Jan 1966, 32-36.

12. Schuermeyer, F. L., Young, C. A., Blasingame, J. M., "Hot Electron Scattering and Photo Emission Measurements on Metal-Insulator-Metal Structure", Technical Report HFAL-TR 68-100, June 1968.

13. Schuermeyer, F. L., Young, C. A., Blasingame, J. M., "Monte Carlo Calculations of Internal Photo Emission Yields in MIM Thin Film Structures", Journal of Applied Physics, Vol 34, Feb 1968, 1791-1796.

14. Chopra, K. L., "Avalanche-Induced Negative Resistance in Thin Oxide Films", Journal of Applied Physics, Vol 36, No. 1, Jan 1965, 184-187.

15. Person, A. D., "Characteristics of Semi-Conductor Glass Switching Memory Diodes", IBM Journal of Research and Development, Vol 13, No. 5, Sep 1969.

16. Fritzsche, H., "Physics of Instabilities in Amorphous Semi-conductors", IBM Journal of Research and Development, Vol 13, No. 5, Sep 1969.

17. Barnett, A. M., "Current Filaments in Semi-conductors", IBM Journal of Research and Development, Vol 13, No. 5, Sep 1969, 522-528.

18. Marley, J. A., Dockerty, R. C., "Electrical Properties of Stannic Oxide Single Crystals", Physical Review, Vol 140, No. 1A 4 Oct 1965, A304-A310.

19. Peterson, A., "The Electrical Properties of Tin Oxide", Doctorial Thesis Rutgers University, Jan 1968.

20. Spence, W., "The UV Absorption Edge of Tin Oxide Thin Film", Journal of Applied Physics, Vol 38, No. 9, Aug 1967, 3767-3770.

21. Huluby, S. A., "The Materials of Thin Film Devices", Electro Technology, Sep 1963, 97-108.

22. Fonstad, C. G., Linz, A., Rediker, R. H., "Vapor Phase Growth of Stannic Oxide Single Crystals", Journal of Electro-Chemical Society, Vol 116, No. 9, Sept 1969, 1269-1271.

23. Fonstad, C. G., Rediker, R., H., "Electrical Properties of High Quality Stannic Oxide Crystals", Journal of Applied Physics, Vol 42, No. 7, June 1971, 2911-2918.

24. Testerman, M. A., Raible, R. W., Gilliland, R. E., Williams, H. R., "Cold Electron Source for Mass Spectrometer Applications", Journal of Applied Physics, Vol 36, No. 9, Sep 1965, 2434-2443.

25. Raja, T. A., Harrell, B. J., "Manifestations of Sustained Secondary Electron Emission from Tin Oxide Films", Journal of Applied Physics, Vol 40, No. 10, Sep 1969, 4213-4214.

26. Soeliner, A. M., Sprouse, J. F., Raja, R. T. H., "Electron Emissions from Regions of High Resistance in Thin Oxide Films", Journal of Applied Physics, Vol 34, No. 3, Feb 1968, 1911-1913.

27. The dielectric strength of the SnO_2 film is not known; and as pointed out by Hickmott (Ref. 4), it is not certain what the definition of dielectric breakdown for these films should be. In any case, the fact that the dielectric strength of the insulators increases with decreasing thickness should help.

28. Hill, J. S., Nicol, W. S., Walton, A. K., Potential Distributions in Surface P-N Junctions, Technical Report No. 71023 Signals Research & Development Establishment (AD 740496), May 1971.

29. Chopra, K. L., Thin Film Phenomena, McGraw-Hill Book Company, New York, N. Y., 1969.

30. Taneo Nishino and Yoshihiro Hamekawa, "Electrical and Optical Properties of Si - SnO_2 Heterojunctions," Japanese Journal of Applied Physics, Vol 9, No. 9, Sep 1970.

APPENDIX A

FINAL TECHNICAL REPORT

on

DEVELOPMENT OF A PROTOTYPE SILICON DEVICE FOR USE AS AN ELECTRON EMITTER

to

BETA INDUSTRIES, INC.

November 22, 1972

by

R. D. Baxter

Pursuant to U.S. Government Contract
DAAK02-72-C-0422

Period of Report: July 15, 1972, to November 22, 1972

BATTELLE
Columbus Laboratories
505 King Avenue
Columbus, Ohio 43201

TABLE OF CONTENTS

FINAL TECHNICAL REPORT

on

DEVELOPMENT OF A PROTOTYPE SILICON DEVICE FOR USE AS AN ELECTRON EMITTER

by

R. D. Baxter

INTRODUCTION

The objective of the research described in this report was the development of techniques for the fabrication of prototype Si device structures in accordance with Beta Industries' design and materials specifications. A critical step in the fabrication of the required device structure was the formation of a relatively deep-etched channel in areas of a single-crystal Si wafer.

The particular technique investigated for this purpose was vapor etching through a window in a thermally grown SiO_2 mask. E-gas (SF_6) was selected as the etchant since, according to the literature[1]*, Si etch rates as high as several μm/min can be obtained at temperatures as low as 950 C. In addition, Si surfaces etched with E-gas were reported to be smooth and free from defects; thermally grown SiO_2 was reported to provide effective masking against etching; and the E-gas itself is both nontoxic and noncorrosive.

The present work indicates, however, that the etch rate of thermally grown SiO_2 upon exposure to E-gas at elevated temperatures is not negligible, being as high as one-tenth of the Si etch rate at 1030 C with an E-gas concentration of 0.5 percent. These results suggest that the maximum channel depth which may reasonably be etched through an SiO_2 mask is limited to a few tens of micrometers, and that successful fabrication of the desired device structure using the E-gas vapor etch would be best accomplished on epitaxial layers rather than bulk Si wafers.

---

* References are listed on page 14.

EXPERIMENTAL DETAILS

The essential elements of the device structure conceived by Beta Industries are sketched in Figure 1. The device may be seen to consist of a single-crystal silicon bar containing two ohmic electrodes separated by an emitter region. The emitter region itself consists of an etched channel which may be filled, or partially filled, with selected insulator-metal combinations.

The basic processing sequence envisioned for achieving the desired structure was as follows

Step 1 - Thermal oxidation of the Si wafer

Setp 2 - Formation of an emitter window in the thermal oxide by photolithographic techniques

Step 3 - Formation of the emitter channel by vapor-phase etching through the oxide mask

Step 4 - Opening of contact windows in the SiO_2

Step 5 - Metallization of contact and channel regions

Step 6 - Removal of excess metallization by photolithograph techniques.

For reasons to be discussed later, the present investigation was confined to processing steps 1 through 3, which were carried out under the experimental conditions listed below.

Oxide Growth

Thermally grown SiO_2 layers were prepared by a dry oxidation process in a conventional, single-wall reactor system. The system consisted of a resistance-heated furnace and Mullite liner, a 60-mm (G.E. 204) fused-quartz oxidation tube, and fused-quartz wafer carrier. Liquified gases were used as sources of oxygen and nitrogen. The inlet lines were of stainless steel, connected to the oxidation tube via Teflon couplings. Both gas lines were filtered.

Preoxidation cleaning of the Si wafers was accomplished using the method described by Kern and Puotinen[2], as follows

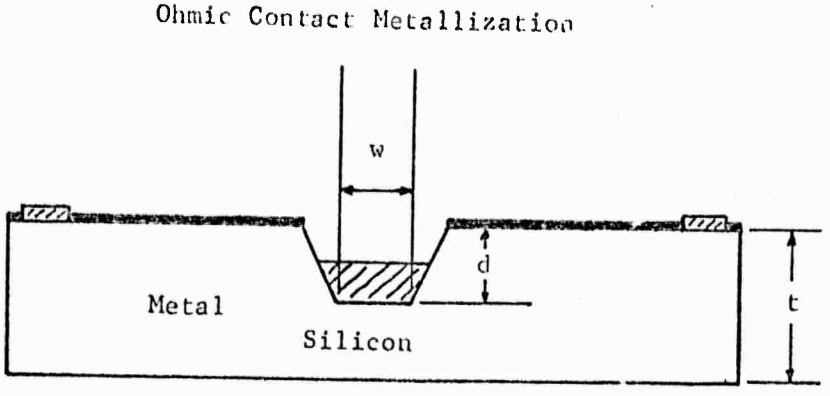

FIGURE 1. ORIGINAL DEVICE GEOMETRY

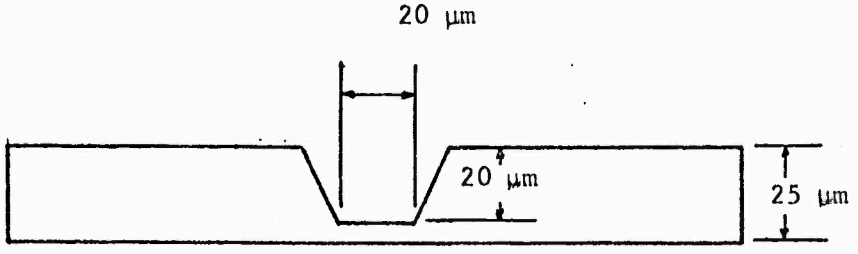

FIGURE 2. MODIFIED DEVICE GEOMETRY

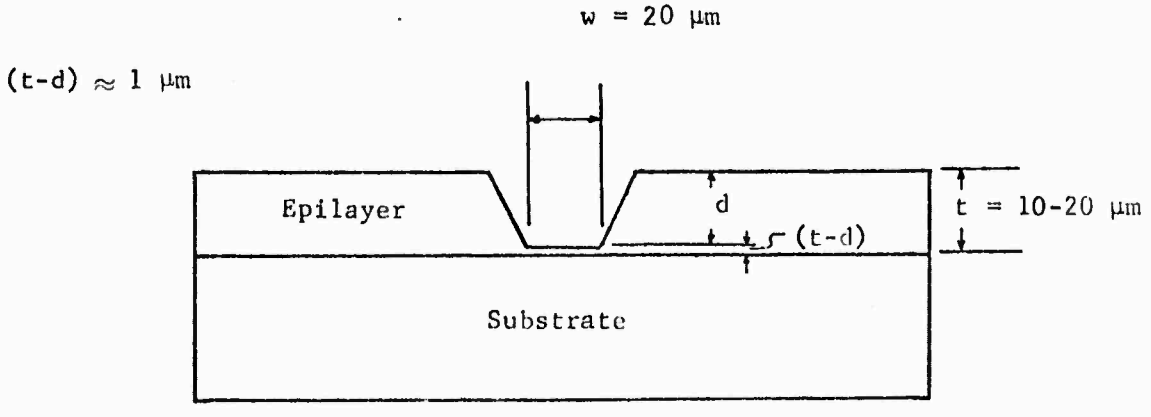

FIGURE 3. DEVICE GEOMETRY FOR EPITAXIAL LAYERS

(1) Degrease in trichloroethylene

(2) Soak for 15 minutes in 5:1:1 solution of H_2O:H_2O_2:HN_4OH at 75-85 C

(3) Quench and rinse in running D.I. water for 5 minutes

(4) Soak for 15 minutes in 6:1:1 solution of H_2O:H_2O_2:HCl at 75-85 C

(5) Quench and rinse in running D.I. water for 10 minutes.

After the final rinse in 18-megohm-cm D.I. water, the wafers were spun dry and immediately loaded into the oxidation tube.

The oxidations were performed in the temperature range of 1000 to 1200 C in pure oxygen for times chosen to yield the desired thickness.

Photolithography

Immediately after oxidation, the wafers were spin-coated at 5000 rpm for 3 sec with a 40-cps solution of KTFR. The coated wafers were then prebaked for 30 min at 80 C and the window pattern formed by exposure with collimated U.V. light through a Cr mask. After pattern development, the photoresist was postbaked for one hour at 150 C, the oxide window was opened with a buffered HF solution, and the photoresist was stripped with hot H_2SO_4.

Vapor Etching

The vapor etching experiments were performed in the system previously employed for wafer oxidation. The E-gas, obtained from Matheson Gas Products, was diluted with He to achieve E-gas volume concentrations in the range 0.05 to 0.5 percent. He flow rates ranging from 2.7 to 24 l/min were employed, corresponding to flow velocities of 1.6 to 14 cm/sec. Etching temperatures in the range 1000-1200 C were employed. In a typical vapor-etch run, the silicon wafer was preheated to the desired temperature in a flow of pure He to achieve thermal equilibrium prior to admission of the E-gas. This preheat time amounted to about 15 min.

After vapor etching for the selected time, which varied from 1 min to 1 hr, the E-gas flow was interrupted and the apparatus flushed with pure He for another 15 min before withdrawing the wafer from the hot zone. Both bare (unoxidized) Si wafers and wafers containing the oxide mask were employed at various stages of the study. In the case of bare wafers, the etch rates under the various etch conditions were determined from the change in thickness of the wafers. In the case of masked wafers, etch rates were determined by Talysurf measurements of the channel depth.

RESULTS AND DISCUSSION

Since the subject program underwent a number of modifications after its initiation, it is necessary to discuss the program and its technical accomplishments in chronological order.

The original device structure conceived by Beta Industries was that shown in Figure 1. The emitter region was to consist of an etched channel having a width, w, equal to the thickness of the silicon bar and a depth, d, euqal to one-half of the bar thickness, t.

By mutual agreement between BCL and Beta Industries, a channel width of 20 μm was selected for the prototype device, thereby implying a total thickness for the finished wafer of about 40 μm. The silicon to be used was comprised of (111)-oriented, p-type, silicon single-crystal wafers supplied by NVL via Beta Industries. The total thickness of a typical as-received wafer was nominally .006 in. or about 150 μm. Therefore, in accordance with the original design, an additional processing step would have involved lapping about 110 μm of material from the back surface of the wafer.

Shortly after initiation of the program, however, estimates of predicted device performance by Beta personnel dictated the modified geometry indicated in Figure 2. Notice that in Figure 2, the design depth of the etched channel has been maintained at 20 μm, while the overall thickness of the Si bar has been reduced to 25 μm. This seemingly slight design modification presented a number of fabrication problems.

Initial experiments showed that vapor-phase etching using E-gas in a He carrier gas could be used to remove up to 20 μm of Si while still maintaining acceptable surface morphology, i.e., surfaces free from excessive pitting and gross irregularities. However, removal of appreciably more Si was always accompanied by increasingly nonuniform etching, substantial rounding off of the wafer edges (the wafers became increasingly dome shaped), and the occurrence of severe surface pitting. The deterioration in surface quality upon vapor etching appeared to be a consequence of both nonoptimum vapor etching conditions, and the quality of the as-received p-type wafers. Cursory examination indicated that flow velocity, temperature, and vapor composition were important factors determining etch rate, etching uniformity, and structure of the etched surface. Clearly, however, a detailed investigation of the effects of these factors was not possible at the funding level provided by the subject contract. Therefore, etching conditions were established essentially by a cut-and-try technique, and there is no assurance that the conditions ultimately employed corresponded to optimum conditions. It was observed, however, during the establishment of at least nominal etching conditions, that the surface of the p-type wafers supplied by NVL deteriorated much more rapidly and to a greater degree during vapor etching than did the surfaces of either (111)- or (100)-oriented 1-ohm-cm n-type wafers etched under identical conditions. It is entirely possible then that the rather heavily doped p-wafers contained precipitates or dislocation clusters which contributed to the observed pitting. Also, the p-wafers were already dome-shaped as received, the thickness of a typical wafer varying by as much as 35 μm from the center to outside edge of the wafer. This domed characteristic was then accentuated during etching.

Whatever the cause, the inability to remove more than a few μm of Si without the attendent loss of surface planarity precluded the use of vapor-etching techniques to thin the wafers to the required 25 μm thickness either before or after channel formation. That is, the results indicated that wafer thinning before channel formation would have resulted in a surface unsuitable for the photolithographic process, and would have

created serious wafer-handling problems during subsequent processing. Wafer-thinning after channel formation would have been similarly fruitless because pits in the channel region or in the back surface opposite the channel region would have destroyed the integrity of the 5-μm-thick Si region bridging the channel and also caused serious vapor-handling problems.

Therefore, at BCL's suggestion, and with Beta Industries' approval, the program was again modified and the remaining BCL effort was devoted to a "one-shot" attempt to achieve the desired device geometry in a silicon epitaxial layer as diagrammed in Figure 3. In view of the preceeding discussion, the use of homoepitaxial or even heteroepitaxial (e.g., silicon on sapphire) layers offers a number of advantages. Referring to Figure 3, the effective device thickness is the thickness, t, of the epitaxial layer, the substrate acting primarily as a supporting structure. Since the epitaxial layer can be grown to the desired thickness, the channel depth, d, may be made arbitrarily close to the film thickness, t, without creating any problems in wafer handling. The design goal for the distance (t-d) was therefore set at approximately 1 μm. Moreover, since no actual wafer thinning is required, the entire etching process may be accomplished through an oxide mask so that no surface degradation occurs outside the channel region.

Investigations utilizing the epilayer approach were performed initially on p/p^+ wafers supplied by Beta Industries and subsequently on portions of n/p and n/p^+ wafers which were obtained by BCL for other intended purposes. The initial results obtained with p/p^+ wafers were only mildly encouraging. Channels of the desired width were readily obtained by vapor etching at 1100 C with $\frac{\text{E-gas}}{\text{He}}$ volume ratios in the range 0.1 to 0.5 percent. However, the maximum channel depth attainable was found to be ≤ 7.5 μm. In addition, after etching, the Si surface in regions of the wafer covered by thermally grown SiO_2 were generally pitted and less smooth than the etched channel, indicating that nonuniform etching was occurring over the regions which were presumed to be protected against the etchant by SiO_2. It was initially thought that these results

occurred owing to undercutting of the thermal oxide in the vicinity of the oxide window and at pinholes, in agreement with the published results of Rai-Choudhury[1]. However, subsequent work revealed the limiting factor to be the nonnegligible etch rate of SiO_2 upon exposure to E-gas at elevated temperatures. Dramatic evidence for the etching of SiO_2 by E-gas was provided when the fused quartz tube used in the etching experiments failed. Examination of the failed tube revealed a noticeable thinning of the tube walls in the failed portion of the tube (i.e., in that portion of the tube exposed to E-gas at elevated temperatures).

Therefore, in the subsequent work with n/p and n/p^+ wafers, channel etching was accomplished in a step-wise manner by exposing the SiO_2 masked wafers to E-gas for successive 1-min intervals. At the end of each 1-min interval, the wafers were withdrawn from the furnace and the decrease in oxide thickness estimated from the oxide color changes. This process was continued until the oxide just disappeared, at which time the channel depth was measured with a Talysurf. The procedure just described was performed at one etching temperature only, 1030 °C, with $\frac{\text{E-gas}}{\text{He}}$ volume ratios of 0.1 and 0.5 percent.

As might be expected in view of the previous discussion, the results indicated a nonnegligible etch rate for the SiO_2 at both E-gas concentrations. Moreover, the etch rates of both Si and SiO_2 increased with increasing E-gas concentration. At an E-gas concentration of 0.1 percent, the Si and SiO_2 etch rates were about 0.67 and 0.05 μm/min respectively, while at a concentration of 0.5 percent, the corresponding Si and SiO_2 etch rates were about 2.0 and 0.25 μm/min. Since the n/p and n/p^+ epiwafers had only been oxidized to t thickness of 0.3 μm, the maximum channel depth which could be achieved amounted to about 4 μm at an E-gas concentration of 0.1 percent and about 2 μm at an E-gas concentration of 0.5 percent.

Figures 4 and 5 are micrographs taken normal to the epilayer surface after formation of a 4-μm-deep channel under vapor etching conditions such that a few hundred angstroms of thermal oxide remained after etching. Figures 6 and 7 are micrographs of similar samples which were

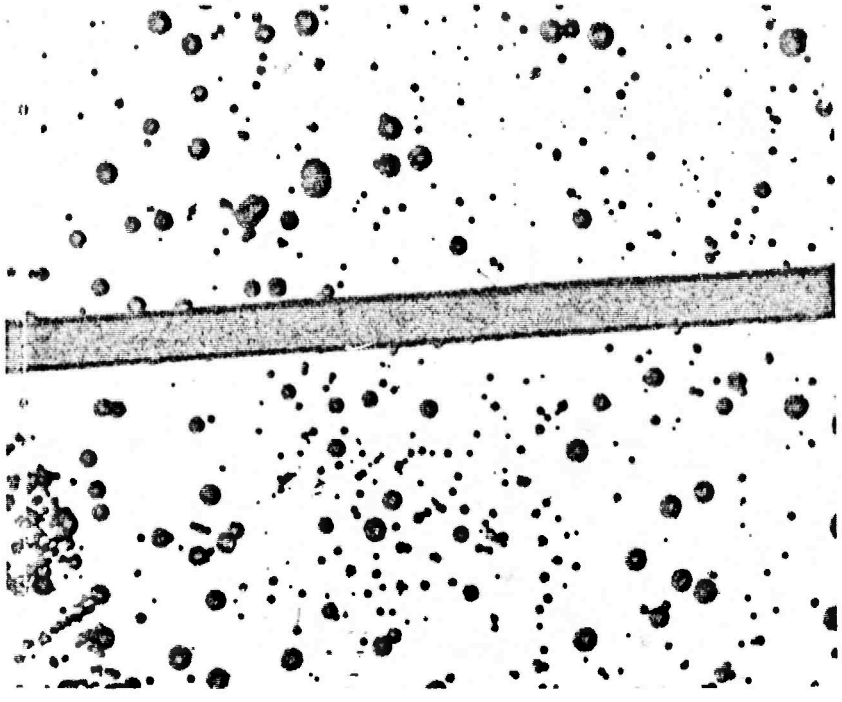

FIGURE 4. CHANNEL REGION OF n/p WAFER: ETCHING TERMINATED PRIOR TO COMPLETE REMOVAL OF SiO_2 LAYER

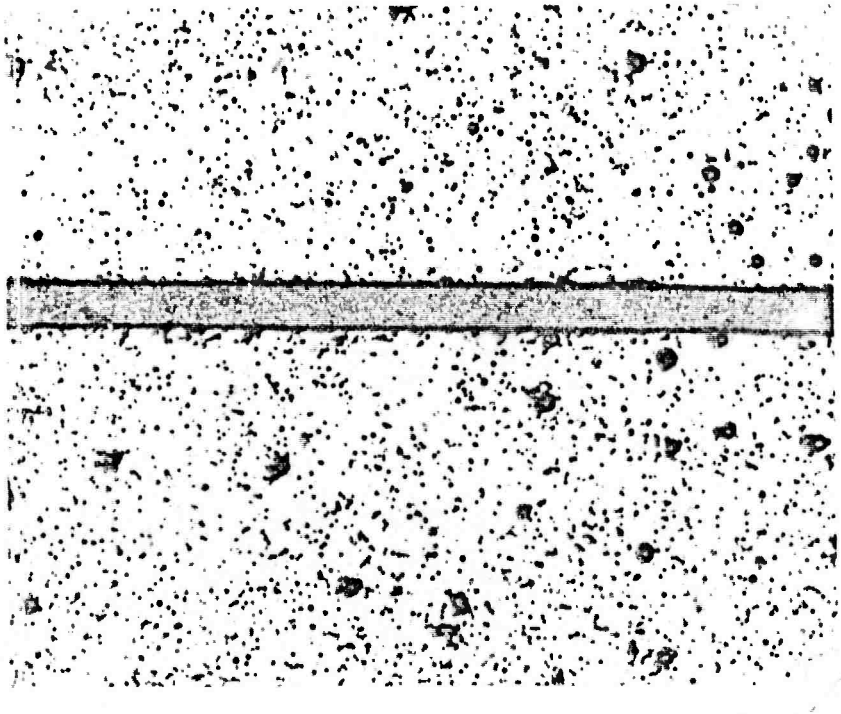

FIGURE 5. CHANNEL REGION OF n/p^+ WAFER: ETCHING TERMINATED PRIOR TO COMPLETE REMOVAL OF SiO_2 LAYER

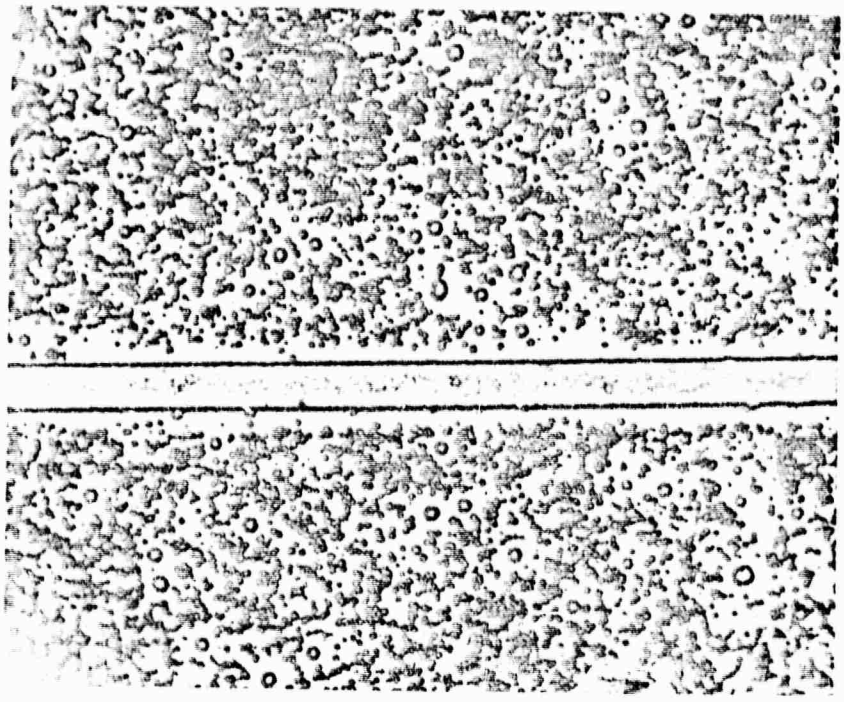

FIGURE 6. CHANNEL REGION OF n/p WAFER: ETCHING CONTINUED AFTER REMOVAL OF SiO_2 LAYER

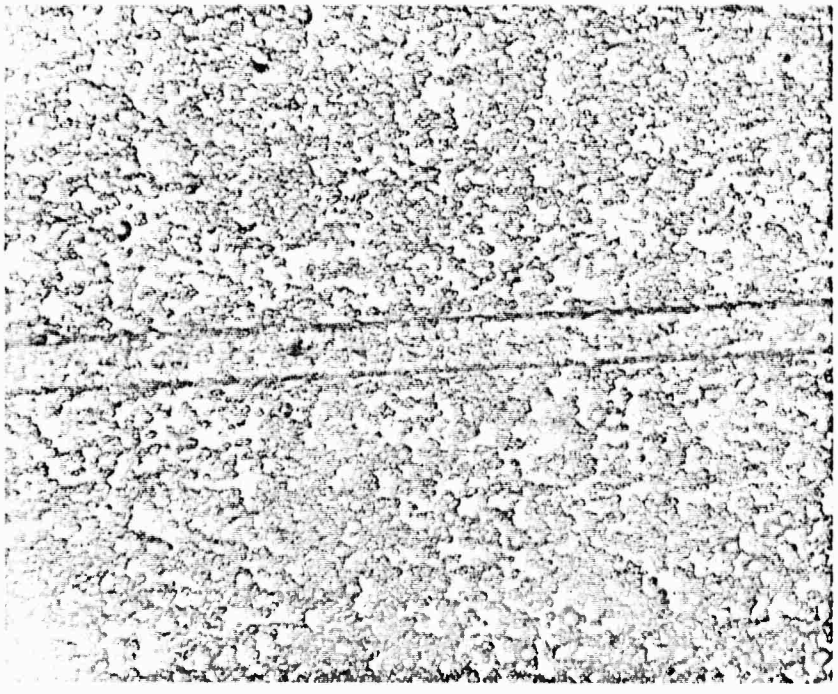

FIGURE 7. CHANNEL REGION OF n/p^+ WAFER: ETCHING CONTINUED AFTER REMOVAL OF SiO_2 LAYER

processed under conditions such that etching continued after the oxide had been completely removed. For the sample corresponding to Figure 6, the etching time and E-gas concentration (2 min at 0.5 percent) was sufficient to remove an additional 4 μm of Si after oxide removal. For the sample corresponding to Figure 7, the time and concentration (5 min at 0.5 percent) were sufficient to remove an additional 10 μm of Si.

A comparison of Figures 4 and 5 with Figures 6 and 7 reveals that an appreciable amount of pitting of the Si surface occurred once the oxide was removed. However, these figures also indicate that no appreciable change in channel geometry occurred during etching of the unprotected Si surface, the etch factor being estimated at about 2 for both sets of samples. Thus, it appears that it is the high oxide etch rate which results in oxide mask failure rather than undercutting at oxide windows or pinholes.

Examination of the samples corresponding to Figures 4-7 after etching also revealed evidence for impurity redistribution during thermal oxidation and/or vapor etching. Figures 4 and 6 correspond to the n/p epi-layer having an epitaxial layer thickness of 10.4 μm. Figures 5 and 7 correspond to the n/p^+ wafer having an epitaxial layer thickness of 19.0 μm. Thermoelectric probing of the surfaces of the samples 4 and 5 indicated that the outer surface of the epitaxial layers were still n-type after channel etching had been accomplished. However, after subsequent removal of an additional 4 μm from the n/p wafer and an additional 10 μm for the n/p^+ wafer, all exposed surfaces of both wafers probed p-type, presumably because of diffusion of p-type impurities from the substrate into the epitaxial layers. Since the length of time the wafers were exposed to elevated temperatures during etching was only a fraction of the time spent at elevated temperatures during oxidation, the redistribution of impurities probably came about during oxidation.

Redistribution of the impurities, then, is another factor which must be overcome before successful device structures can be achieved by the vapor-etch technique.

CONCLUSIONS AND RECOMMENDATIONS

Although no devices of the desired geometry were successfully fabricated during the subject effort, the results indicate that the fabrication of structures possessing channel depths up to about 10 μm, is certainly feasible. In particular, the results indicate that the primary limitation on the depth of a channel which may be vapor etched through an SiO_2 mask is the thickness of the mask itself. The SiO_2 etch-rate determinations accomplished in the present work indicate that the successful achievement of a 10-μm channel depth at an E-gas concentration of 0.1 percent and at a temperature of 1030 C would require a minimum oxide thickness of about 0.75 μm. At an E-gas concentration of 0.5 percent, also at a temperature of 1030 C, the minimum oxide thickness required would be about 1.0 μm. In addition, it would be desirable to have at least a few thousand angstroms of oxide remaining after vapor etching. This remaining oxide would be used for a mask for channel and contact metallization. Thus, an optimum oxide thickness would more likely be in the range of 1-2 μm. For deeper channels, the required oxide thickness would, of course, be correspondingly thicker. Ultimately, the limitation on channel depth will be provided by the maximum oxide thickness amenable to photolithographic techniques. For oxide thicknesses in the range 1-2 μm, standard photoresist techniques can be employed so that no particular difficulty would be expected in the fabrication of 10-μm-deep channels. However, a 10-μm-deep channel would probably have application only in epitaxial layer structures in which the active (epitaxial) layer thickness was $\leq$ 12 μm. In order to avoid the problem of impurity redistribution during the relatively long time and high temperature required to grow a thermal oxide 1-2 μm thick, it would be preferable to employ a chemically deposited oxide. Deposition of an SiO_2 layer by oxidation of silane, for example, can be carried out at temperatures of about 350 C. At this temperature little interdiffusion of impurities between the substrate and epilayer would be expected. Thus, the following processing technique, capable of producing 10-μm-deep channels in silicon epitaxial layers while at the same time providing adequate surface protection, is recommended

Step 1 - Deposit 1.5 μm of SiO_2 by oxidation of silane

Step 2 - Open oxide window in channel region by photolithographic techniques

Step 3 - Vapor etch channel to depth of 10 μm

Step 4 - Open contact windows in remaining oxide

Step 5 - Metallize channel and contact regions

Step 6 - Remove excess metallization by photolithographic techniques.

REFERENCES

1. P. Rai-Choudhury, "Sulfur Hexflouride as an Etchant for Silicon," J. Electrochem Soc 118, 266 (1971).

2. Werner Kern and David A. Puotinen, "Cleaning Solutions Based on Hydrogen Peroxide for use in Silicon Semiconductor Technology," RCA Review 31, 187 (1970).

Unclassified

Security Classification

DOCUMENT CONTROL DATA - R & D

(Security classification of title, body of abstract and indexing annotation must be entered when the overall report is classified)

1. ORIGINATING ACTIVITY *(Corporate author)*

Beta Industries, Inc.
2763 Culver Avenue
Dayton, Ohio 45429

2a. REPORT SECURITY CLASSIFICATION

Unclassified

2b. GROUP

3. REPORT TITLE

DEVELOPMENT OF VARIABLE AFFINITY BARRIER PHOTOEMITTER

4. DESCRIPTIVE NOTES *(Type of report and inclusive dates)*

FINAL TECHNICAL REPORT - 20 April 1972 through 20 November 1972

5. AUTHOR(S) *(First name, middle initial, last name)*

John L. Mize

6. REPORT DATE	7a. TOTAL NO. OF PAGES	7b. NO. OF REFS
October 1973	71	30

8a. CONTRACT OR GRANT NO.	9a. ORIGINATOR'S REPORT NUMBER(S)
DAAK02-72-C-0422	225
b. PROJECT NO. ARPA No. 2167	
c.	9b. OTHER REPORT NO(S) *(Any other numbers that may be assigned this report)*
d.	

10. DISTRIBUTION STATEMENT

Distribution limited to U. S. Government Agencies only, ~~due to specialized fabrication, processing and manufacturing techniques,~~ effective date of this report. Other request for this document must be referred to Director, Night Vision Laboratory, Fort Belvoir, Virginia 22060.

11. SUPPLEMENTARY NOTES	12. SPONSORING MILITARY ACTIVITY
	Advanced Research Projects Agency Equipment Research and Development Center Research and Development Office Fort Belvoir, Virginia 22060

13. ABSTRACT

Cold cathode emission was obtained for devices fabricated using Si - SnO_2 hetero-junctions. Due to excessive heating the devices failed before photo measurements could be made.

Devices fabricated by "etching" silicon either single crystal or expitaxial exhibited no electron emission.

DD FORM 1 NOV 65 1473

Unclassified

Security Classification

14. KEY WORDS	LINK A		LINK B		LINK C	
	ROLE	WT	ROLE	WT	ROLE	WT